International Journal of Engineering Science 92 (2015) 63–82

Contents lists available at ScienceDirect

International Journal of Engineering Science

journal homepage: www.elsevier.com/locate/ijengsci

Dispersion of Rayleigh waves in weakly anisotropic media with vertically-inhomogeneous initial stress

Kazumi Tanuma [a,*], Chi-Sing Man [b], Yue Chen [b]

[a] Department of Mathematics, Faculty of Science and Technology, Gunma University, Kiryu 376-8515, Japan
[b] Department of Mathematics, University of Kentucky, Lexington, KY 40506-0027, USA

ARTICLE INFO

Article history:
Received 13 January 2015
Accepted 11 March 2015

Keywords:
Rayleigh waves
Vertical inhomogeneity
Dispersion
Initial stress
Weakly anisotropic media
Surface impedance

ABSTRACT

Herein we present a procedure by which a high-frequency asymptotic formula can be derived for dispersion relations of Rayleigh waves that propagate in various directions along the free surface of a vertically-inhomogeneous, prestressed, and generally anisotropic half-space. The procedure is based on three assumptions, namely: (i) the incremental elasticity tensor of the material half-space can be written as the sum of a homogeneous isotropic part $\mathbb{C}^{\rm iso}$ and a depth-dependent perturbative part $\mathbb{A}$; (ii) at the free surface both the initial stress and $\mathbb{A}$ are small as compared with $\mathbb{C}^{\rm iso}$; (iii) the mass density, the initial stress, and $\mathbb{A}$ are smooth functions of depth from the free surface. We derive formulas and Lyapunov-type equations that can iteratively deliver each term of an asymptotic expansion of the surface impedance matrix, which leads to the aforementioned high-frequency asymptotic formula for Rayleigh-wave dispersion. As illustration we consider a thick-plate sample of AA 7075-T651 aluminum alloy, which has one face treated by low plasticity burnishing that induced a (depth-dependent) prestress at and immediately beneath the treated surface. We model the sample as a prestressed, weakly-textured orthorhombic aggregate of cubic crystallites and work out explicitly, up to the third order, the dispersion relations that pertain to Rayleigh waves propagating in several directions along the treated face of the sample.

1. Introduction

Recently Man, Nakamura, Tanuma, and Wang (2015) developed a general procedure, under the framework of linear elasticity with initial stress (Biot, 1965; Hoger, 1986; Man & Carlson, 1994; Man & Lu, 1987), for obtaining a high-frequency asymptotic formula for the dispersion of Rayleigh waves propagating in a vertically-inhomogeneous, prestressed and anisotropic medium. That work was meant to serve as the mathematical foundation for a nondestructive measurement technique to monitor the retention of protective surface and subsurface compressive stresses which are put in metal parts (e.g., critical components of aircraft engines) by surface treatments for fatigue-life enhancement. The theory in Man et al. (2015) does not consider the effects of surface roughness on Rayleigh-wave dispersion; it covers only surface treatments (e.g., low plasticity burnishing (LPB), which leaves a mirror-smooth surface finish) where such effects can be ignored. On the other hand, that theory is developed with the constitutive equation in linear elasticity with initial stress put in its most general form, which makes derivation of explicit dispersion relations difficult.

* Corresponding author. Tel.: +81 277 301915; fax: +81 277 301954.
E-mail addresses: tanuma@gunma-u.ac.jp (K. Tanuma), cman@uky.edu (C.-S. Man), chenyue0715@uky.edu (Y. Chen).

http://dx.doi.org/10.1016/j.ijengsci.2015.03.001
0020-7225/

Here we adapt the general procedure in Man et al. (2015) to the case where the incremental elasticity tensor $\mathbb{L}$ can be written as the sum of an isotropic part $\mathbb{C}^{\rm Iso}$ and a perturbative part $\mathbb{A}$. Under a Cartesian coordinate system where the material medium occupies the half-space $x_3 \leqslant 0$, the perturbative part $\mathbb{A}(\cdot)$, the initial stress $\mathring{\boldsymbol{T}}(\cdot)$, and the mass density $\rho(\cdot)$ are assumed to be smooth functions of x_3. Moreover, at the free surface $x_3 = 0$ of the material medium $\mathbb{A}(0)$ and $\mathring{\boldsymbol{T}}(0)$ are assumed to be sufficiently small as compared with $\mathbb{C}^{\rm Iso}$ that, for all expressions and formulas which depend on $\mathbb{A}(0)$ and $\mathring{\boldsymbol{T}}(0)$, it suffices to keep only those terms linear in the components of these tensors. Under this setting, after outlining some preliminaries in Section 2, we derive in Sections 3–5 specific formulas with which the procedure presented in Man et al. (2015) can be implemented to solve the direct problem of deriving high-frequency asymptotic formulas for dispersion relations that pertain to Rayleigh waves with various propagation directions. Once dispersion curves can be generated when requisite data on material and stress are given, the inverse problem of inferring stress retention from Rayleigh-wave dispersion can be attacked by an iterative approach in further studies.

In Section 6, we present an illustrative example where we derive Rayleigh-wave dispersion relations for a thick-plate sample of an AA 7075-T651 aluminum alloy that carries a prestress induced by prior LPB-treatment. The sample is modeled as a weakly-textured orthorhombic aggregate of cubic crystallites. The prestress in the sample was ascertained by destructive means (X-ray diffraction and hole-drilling), and so were the relevant texture coefficients (X-ray diffraction). To shed light on how crystallographic texture would affect the dispersion relations, we prescribe two other textures to the sample and repeat the calculations with the prestress and material parameters unchanged.

2. Preliminaries

In a Cartesian coordinate system let (x_1, x_2, x_3) be the Cartesian coordinates of place $\mathbf{x}$, and let $\boldsymbol{u} = \boldsymbol{u}(\mathbf{x}) = (u_1, u_2, u_3)$ be the displacement at $\mathbf{x}$ pertaining to the superimposed small elastic motion. We work in the theoretical context of linear elasticity with initial stress, under which the constitutive equation can be put in the form (cf. Man & Carlson (1994), Man & Lu (1987))

$$\boldsymbol{S} = \mathring{\boldsymbol{T}} + \boldsymbol{H}\,\mathring{\boldsymbol{T}} + \mathbb{L}[\boldsymbol{E}]; \tag{1}$$

here $\boldsymbol{S} = (S_{ij})$ is the first Piola–Kirchhoff stress, $\mathring{\boldsymbol{T}} = (\mathring{T}_{ij})$ the initial stress, $\boldsymbol{H} = (\partial u_i/\partial x_j)$ the displacement gradient pertaining to the superimposed small elastic motion, and $\boldsymbol{E} = (\boldsymbol{H} + \boldsymbol{H}^T)/2$ the corresponding infinitesimal strain, where the superscript T denotes transposition; $\mathbb{L}$ is the incremental elasticity tensor which, when regarded as a fourth-order tensor on symmetric tensors, has its components L_{ijkl} $(i,j,k,l = 1,2,3)$ satisfying the major and minor symmetries.

We choose the Cartesian coordinate system so that the material half-space occupies the region $x_3 \leqslant 0$ whereas the 1- and 2-axes are chosen arbitrarily. In this paper we assume that the initial stress $\mathring{\boldsymbol{T}} = \mathring{\boldsymbol{T}}(x_3)$, the incremental elasticity tensor $\mathbb{L} = \mathbb{L}(x_3)$, and the mass density $\rho = \rho(x_3)$ are smooth functions of the coordinate x_3 $(x_3 \leqslant 0)$. Here and hereafter we use the term "smooth function" to denote an infinitely differentiable function all of whose derivatives are bounded and continuous. We assume that the initial stress $\mathring{\boldsymbol{T}}$ satisfies the equation of equilibrium $\operatorname{div} \mathring{\boldsymbol{T}} = \boldsymbol{0}$, and that the surface $x_3 = 0$ of the half-space is free of traction, which implies that the components $\mathring{T}_{i3}(x_3)$ $(i = 1,2,3)$ of $\mathring{\boldsymbol{T}}$ vanish at the surface $x_3 = 0$. We call $-x_3 \geqslant 0$ the depth of place $\mathbf{x}$ beneath the free surface $x_3 = 0$.

In what follows we suppose that $\mathbb{L}$ can be written as a sum of two terms: a principal part $\mathbb{C}^{\rm Iso}$ which is *homogeneous* and isotropic, and a perturbative part $\mathbb{A} = \mathbb{A}(x_3)$ which is a smooth function of x_3 $(x_3 \leqslant 0)$ and is generally anisotropic. Then $\mathbb{L}$ can be expressed as a fourth-order tensor on symmetric tensors $\boldsymbol{E}$ in the form

$$\mathbb{L}[\boldsymbol{E}] = \mathbb{C}^{\rm Iso}[\boldsymbol{E}] + \mathbb{A}[\boldsymbol{E}] = \lambda(\operatorname{tr}\boldsymbol{E})\mathbf{I} + 2\mu\boldsymbol{E} + \mathbb{A}[\boldsymbol{E}], \tag{2}$$

where $\mathbf{I}$ is the identity matrix, λ and μ are the Lamé constants that pertain to $\mathbb{C}^{\rm Iso}$, and $\mathbb{A}$ can be written under the Voigt notation as a 6×6 symmetric matrix $(a_{rs}(x_3))$ with its components a_{rs} being smooth functions of x_3 $(x_3 \leqslant 0)$. In the present study we adopt the following basic assumption:

(*) At the free surface $x_3 = 0$, the perturbative part $\mathbb{A}$ of $\mathbb{L}$ and the initial stress $\mathring{\boldsymbol{T}}$ are sufficiently small as compared with the isotropic part $\mathbb{C}^{\rm Iso}$ of $\mathbb{L}$ (i.e., $\|\mathring{\boldsymbol{T}}(0)\| \ll \|\mathbb{C}^{\rm Iso}\|, \|\mathbb{A}(0)\| \ll \|\mathbb{C}^{\rm Iso}\|$, where $\|\cdot\|$ denotes the Euclidean norm) that for all expressions and formulas which depend on $\mathbb{A}(0)$ and $\mathring{\boldsymbol{T}}(0)$ it suffices to keep only those terms linear in the components of these tensors.

Throughout this paper, we do not put any condition on the x_3-derivatives of $\mathbb{A}(x_3)$ and of $\mathring{\boldsymbol{T}}(x_3)$ at $x_3 = 0$.

Substituting the componentwise expression of (1) into the equations of motion with zero body force, we obtain elastic wave equations of the form

$$\rho\,\frac{\partial^2}{\partial t^2}\,u_i \;=\; \sum_{j,k,l=1}^{3} \frac{\partial}{\partial x_j}\left(B_{ijkl}\,\frac{\partial u_k}{\partial x_l}\right), \quad i = 1,2,3, \tag{3}$$

where t denotes the time,

$$B_{ijkl} = B_{ijkl}(x_3) = \delta_{ik}\overset{\circ}{T}_{jl}(x_3) + L_{ijkl}(x_3) \tag{4}$$

are the effective elastic coefficients, and δ_{ik} is the Kronecker delta.

We consider Rayleigh waves propagating in a given direction along the traction-free surface of the aforementioned vertically-inhomogeneous, anisotropic and prestressed half-space $x_3 \leqslant 0$. These waves are described as a surface-wave solution to (3) in $x_3 \leqslant 0$ which is time-harmonic, has the form

$$\boldsymbol{u} = (u_1, u_2, u_3) = e^{-ik(x_1\eta_1 + x_2\eta_2 - vt)}\ \mathbf{a}(\mathbf{x}, \eta_1, \eta_2, v, k), \tag{5}$$

and satisfies the traction-free boundary condition

$$\boldsymbol{s}_{\mathbf{n}}(\boldsymbol{u})|_{x_3=0} = \left(\sum_{r,s=1}^{3} B_{p3rs}\frac{\partial u_r}{\partial x_s}\right)_{p\downarrow 1,2,3}\Bigg|_{x_3=0} = \mathbf{0}. \tag{6}$$

Here $i = \sqrt{-1}$, k is the wave number, $\boldsymbol{\eta} = (\eta_1, \eta_2, 0)$ is the direction of wave propagation on the surface, v is the phase velocity in the subsonic range to be determined, and $\mathbf{a}(\mathbf{x}, \eta_1, \eta_2, v, k)$ is the complex-valued polarization vector which decays exponentially as $x_3 \longrightarrow -\infty$.

Under the assumption on existence of Rayleigh waves Man et al. (2015) recently derived a high-frequency asymptotic formula

$$v_R = v_R(k) = v_0 + v_1 k^{-1} + v_2 k^{-2} + v_3 k^{-3} + \cdots \tag{7}$$

which, for a large wave number k, expresses the phase velocity v_R of the Rayleigh waves in question in terms of $\mathbb{L}(x_3), \overset{\circ}{\boldsymbol{T}}(x_3), \rho(x_3)$ at $x_3 = 0$ and their first and higher-order x_3-derivatives at $x_3 = 0$. They developed a procedure which can deliver an expression for each term v_i $(i = 0, 1, 2, \ldots)$. The asymptotic formula for v_R thus gives a characterization of the frequency-dependence of the Rayleigh-wave velocity, i.e., the dispersion of Rayleigh waves, as caused by the vertical inhomogeneity of the medium.

The surface impedance matrix $\mathbf{Z}(v) = \mathbf{Z}(v, \boldsymbol{\eta}, k)$ is a 3×3 matrix that expresses a linear relationship between the displacements at the surface on which surface waves propagate with phase velocity v and the surface tractions needed to sustain them;

$$\boldsymbol{s}_{\mathbf{n}}(\boldsymbol{u})|_{x_3=0} = \mathbf{Z}(v)\,(\boldsymbol{u}|_{x_3=0}), \tag{8}$$

where $\boldsymbol{u}$ is the solution (5). By Section 5 of Man et al. (2015), $\mathbf{Z}(v)$ admits an asymptotic expansion

$$\mathbf{Z}(v) = k\mathbf{Z}_0(v) + \mathbf{Z}_1(v) + k^{-1}\mathbf{Z}_2(v) + k^{-2}\mathbf{Z}_3(v) + \cdots; \tag{9}$$

here $k\mathbf{Z}_0(v)$ is nothing but the surface impedance matrix[1] of the comparative homogeneous elastic half-space which has its incremental elasticity tensor, mass density, and initial stress equal to $\mathbb{L}(0), \rho(0)$, and $\overset{\circ}{\boldsymbol{T}}(0)$, respectively. It is proved in Man et al. (2015) that each $\mathbf{Z}_n(v)$ $(n = 0, 1, 2, \ldots)$ is Hermitian, i.e., $\mathbf{Z}_n(v) = \overline{\mathbf{Z}_n(v)}^T$, where the overbar denotes complex conjugation.

The surface impedance matrix plays a crucial role on the procedure which delivers each term of the asymptotic expansion (7). It follows from (6) and (8) that the matrix $\mathbf{Z}(v)$ has a non-trivial null space in a three-dimensional complex linear space at the phase velocity of the Rayleigh waves v_R. This leads us to the asymptotic representation of a secular equation for v_R

$$\det\left[\mathbf{Z}_0(v) + \mathbf{Z}_1(v)k^{-1} + \mathbf{Z}_2(v)k^{-2} + \mathbf{Z}_3(v)k^{-3} + \cdots\right] = 0, \tag{10}$$

from which the high-frequency asymptotic formula (7) can be derived by a simple routine through the implicit function theorem (cf. Section 6 of Man et al. (2015)).

In this paper, under the assumption (*) we develop a perturbation method for determining each term v_i $(i = 0, 1, 2, \ldots)$ in (7). Henceforth, without loss of generality we consider Rayleigh waves which propagate along the surface of the prestressed half-space $x_3 \leqslant 0$ in the direction of the (arbitrarily-chosen) 2-axis ($\boldsymbol{\eta} = (0, 1, 0)$).

3. Surface impedance matrix of weakly-anisotropic homogeneous elastic half-space

In what follows, by the comparative homogeneous elastic half-space $x_3 \leqslant 0$ we mean that which has the incremental elasticity tensor $\mathbb{L}$, mass density ρ, and initial stress $\overset{\circ}{\boldsymbol{T}}$ given by

[1] Note that in the literature on the Stroh formalism for homogeneous elastic media it is $\mathbf{Z}_0(v)$ which is usually called the "surface impedance matrix"; see, for example, Lothe and Barnett (1976), Chapter 7 of Chadwick and Smith (1977), Chapter 12 of Ting (1996) and Definition 4.3 of Tanuma, Man, and Du (2013).

$$\mathbb{L} = \mathbb{L}(0) = \mathbb{C}^{\mathrm{Iso}} + \mathbb{A}(0), \tag{11}$$

$\rho = \rho(0)$, and $\overset{\circ}{\boldsymbol{T}} = \overset{\circ}{\boldsymbol{T}}(0)$, respectively. The constitutive equation in this homogeneous half-space is then

$$\boldsymbol{S} = \overset{\circ}{\boldsymbol{T}}(0) + \boldsymbol{H}\,\overset{\circ}{\boldsymbol{T}}(0) + \mathbb{C}^{\mathrm{Iso}}[\boldsymbol{E}] + \mathbb{A}(0)[\boldsymbol{E}].$$

We recall that the components $\overset{\circ}{T}_{i3}(x_3)$ $(i = 1, 2, 3)$ of $\overset{\circ}{\boldsymbol{T}}(x_3)$ vanish at the traction-free surface $x_3 = 0$.

In this section we give a formula for $\mathbf{Z}_0(v)$ which appears as the dominant term in the asymptotic expansion (9), i.e., a formula for the surface impedance matrix that pertains to surface waves which propagate in the direction of the 2-axis along the surface of the comparative homogeneous elastic half-space $x_3 \leqslant 0$. Under assumption (*), we are concerned only with the terms in $\mathbf{Z}_0(v)$ up to those linear in $\overset{\circ}{\boldsymbol{T}}(0)$ and $\mathbb{A}(0)$, which leads us to write

$$\mathbf{Z}_0(v) \approx \mathbf{Z}_0^{\mathrm{Iso}}(v) + \mathbf{Z}_0^{\mathrm{Ptb}}(v). \tag{12}$$

Here and hereafter we use the notation $\approx$ to indicate that we are retaining terms up to those linear in $\mathbb{A}(0)$ and $\overset{\circ}{\boldsymbol{T}}(0)$ and that we are neglecting the higher order terms. $\mathbf{Z}_0^{\mathrm{Iso}}(v)$ is of zeroth order in $\overset{\circ}{\boldsymbol{T}}(0)$ and $\mathbb{A}(0)$, whereas $\mathbf{Z}_0^{\mathrm{Ptb}}(v)$ is of first order in $\overset{\circ}{\boldsymbol{T}}(0)$ and $\mathbb{A}(0)$. Note that $k\mathbf{Z}_0^{\mathrm{Iso}}(v)$ is the surface impedance matrix pertaining to a homogeneous isotropic elastic half-space with constitutive equation $\boldsymbol{S} = \mathbb{C}^{\mathrm{Iso}}[\boldsymbol{E}]$ and with density $\rho = \rho(0)$.

The Hermitian matrix $\mathbf{Z}_0^{\mathrm{Iso}}(v)$ has a well-known formula (cf. for example, Section 12.10 of Ting (1996)), which is given by

Proposition 3.1.

$$\mathbf{Z}_0^{\mathrm{Iso}}(v) \;=\; \overline{\mathbf{Z}_0^{\mathrm{Iso}}(v)}^{T} \;=\; \begin{pmatrix} s_{11} & 0 & 0 \\ 0 & s_{22} & -is_{23} \\ 0 & is_{23} & s_{33} \end{pmatrix}, \tag{13}$$

where

$$s_{11} = \sqrt{\mu(\mu - V)}, \quad s_{22} = \frac{\sqrt{\mu(\lambda + 2\mu - V)}\left(\sqrt{\mu(\lambda + 2\mu)} + \sqrt{(\mu - V)(\lambda + 2\mu - V)}\right)}{\lambda + 3\mu - V},$$

$$s_{33} = \frac{\sqrt{(\lambda + 2\mu)(\mu - V)}\left(\sqrt{\mu(\lambda + 2\mu)} + \sqrt{(\mu - V)(\lambda + 2\mu - V)}\right)}{\lambda + 3\mu - V},$$

$$s_{23} = \frac{1}{\lambda + 3\mu - V}\left(\mu(\lambda + 4\mu - 2V) - \sqrt{\mu(\lambda + 2\mu)(\mu - V)(\lambda + 2\mu - V)}\right), \quad V = \rho(0)\,v^2, \quad i = \sqrt{-1}$$

and λ and μ are the Lamé constants that pertain to $\mathbb{C}^{\mathrm{iso}}$.

Under assumption (*), we apply a perturbation argument to the integral representation of $\mathbf{Z}_0(v)$ in the subsonic range (cf. Lothe & Barnett (1976) and Sections 4.D and 7.D of Chadwick & Smith (1977))

$$\mathbf{Z}_0(v) = \mathbf{S}_2^{-1} + i\mathbf{S}_2^{-1}\mathbf{S}_1,$$

where

$$\mathbf{S}_1 = \frac{1}{2\pi}\int_{-\pi}^{\pi} -\mathbf{T}_0(\phi)^{-1}\mathbf{R}_0(\phi)^T\,d\phi, \quad \mathbf{S}_2 = \frac{1}{2\pi}\int_{-\pi}^{\pi} \mathbf{T}_0(\phi)^{-1}\,d\phi,$$

$$\mathbf{R}_0(\phi) = \left(\sum_{j,l=2}^{3} B_{ijkl}(0)(\mathbf{m}\cos\phi + \mathbf{n}\sin\phi)_j(-\mathbf{m}\sin\phi + \mathbf{n}\cos\phi)_l\right) + \rho(0)\,v^2\cos\phi\,\sin\phi\,\mathbf{I},$$

$$\mathbf{T}_0(\phi) = \left(\sum_{j,l=2}^{3} B_{ijkl}(0)(-\mathbf{m}\sin\phi + \mathbf{n}\cos\phi)_j(-\mathbf{m}\sin\phi + \mathbf{n}\cos\phi)_l\right) - \rho(0)\,v^2\sin^2\phi\,\mathbf{I}$$

and $\mathbf{m} = (0, 1, 0)$ is the propagation direction of the surface waves in question and $\mathbf{n} = (0, 0, 1)$ is the unit outward normal of the boundary $x_3 = 0$ of the material half-space, to obtain an explicit formula for $\mathbf{Z}_0^{\mathrm{Ptb}}(v)$ (cf. the methods in Sections 6 and 7 of Tanuma & Man (2002), Sections 6 and 7 of Tanuma & Man (2008), and Section 4 of Tanuma et al. (2013)):

Proposition 3.2.

$$\mathbf{Z}_0^{\mathrm{Ptb}}(v) = \overline{\mathbf{Z}_0^{\mathrm{Ptb}}(v)}^{T} = \begin{bmatrix} \ell_{11}(a_{55}, a_{66}, \overset{\circ}{T}_{22}) & \ell_{12}^{\mathrm{R}}(a_{26}, a_{36}, a_{45}) + i\ell_{12}^{\mathrm{I}}(a_{25}, a_{35}, a_{46}) & \ell_{13}^{\mathrm{R}}(a_{25}, a_{35}, a_{46}) + i\ell_{13}^{\mathrm{I}}(a_{26}, a_{36}, a_{45}) \\ * & \ell_{22}(a_{22}, a_{23}, a_{33}, a_{44}, \overset{\circ}{T}_{22}) & \ell_{23}^{\mathrm{R}}(a_{24}, a_{34}) + i\ell_{23}^{\mathrm{I}}(a_{22}, a_{23}, a_{33}, a_{44}, \overset{\circ}{T}_{22}) \\ * & * & \ell_{33}(a_{22}, a_{23}, a_{33}, a_{44}, \overset{\circ}{T}_{22}) \end{bmatrix}, \tag{14}$$

where the diagonal components ℓ_{ii} $(i=1,2,3)$ *and* $\ell^{\mathrm{R}}_{ij}, \ell^{\mathrm{I}}_{ij}$ $((i,j)=(1,2),(1,3),(2,3))$ *in the off-diagonal components are real-valued linear functions of their arguments whose coefficients are given explicitly in terms of the Lamé constants* λ, μ *and* $V=\rho(0)\,v^2$*, and the label "*$*$*" in the* (j,i) *component of the matrix denotes the complex conjugate of the* (i,j) *component of the matrix* $((i,j)=(1,2),(1,3),(2,3))$*. All the components of* $\mathring{\boldsymbol{T}}$ *and* $\mathbb{A}$ *in the preceding formula denote their values at* $x_3=0$*. The formulas for the aforementioned linear functions are given in Appendix A.*

Remark 3.3. For a weakly-anisotropic homogeneous elastic half-space, Song and Fu (2007) obtained a general formula for the first-order perturbation of the surface impedance matrix at the Rayleigh-wave velocity in the process of deriving a first-order correction to the Rayleigh-wave velocity. The formula ((2.6) therein) is written in an integral form over a semi-infinite interval whose integrand involves the eigenvalues and eigenvectors of Stroh's eigenvalue problem for the base material. We observe that formula (14) together with those in Appendix A can be derived from Song and Fu's formula (2.6) by keeping the velocity in their formula free and not fixed at the Rayleigh-wave velocity.

4. Lower-order terms of the asymptotic expansion of surface impedance matrix

Now we turn to study the surface impedance matrix $\mathbf{Z}(v)$ that pertains to surface waves which propagate in the direction of the 2-axis along the surface of the vertically-inhomogeneous, anisotropic and prestressed elastic half-space $x_3 \leqslant 0$. Recall that the constitutive equation is expressed by (1), where the incremental elasticity tensor has the form (2), and the mass density is given by $\rho(x_3)$. Let $\mathbf{Q}$, $\mathbf{R}$ and $\mathbf{T}$ be 3×3 real matrices given by

$$\mathbf{Q}=\mathbf{Q}(x_3,v)=\big(B_{i2k2}(x_3)-\rho(x_3)\,v^2\delta_{ik}\big),\quad \mathbf{R}=\mathbf{R}(x_3)=(B_{i2k3}(x_3)),\quad \mathbf{T}=\mathbf{T}(x_3)=(B_{i3k3}(x_3)), \tag{15}$$

where $B_{ijkl}=B_{ijkl}(x_3)$ are the effective elastic coefficients (4). Let $\mathbf{Q}_n, \mathbf{R}_n, \mathbf{T}_n$ and $\mathbf{S}_n$ $(n=0,1,2,\ldots)$ be the coefficients in the Taylor expansions of $\mathbf{Q}$, $\mathbf{R}$, $\mathbf{T}$ and $\mathbf{T}^{-1}$ at $x_3=0$, respectively.

According to the arguments in Sections 3 and 5 of Man et al. (2015), each lower-order term in (9), i.e., each of the 3×3 matrices $\mathbf{Z}_n(v)$ $(n=1,2,3,\ldots)$, is obtained by solving some systems of Lyapunov-type equations. From Eqs. (58) and (101) of Man et al. (2015) we get

$$\mathbf{Z}_n(v)=i\boldsymbol{G}_0^{(-n)}\quad (n=1,2,3,\ldots), \tag{16}$$

where the 3×3 matrix $\boldsymbol{G}_0^{(-n)}$ is the last term of a sequence of 3×3 matrices $\left\{\boldsymbol{G}_n^{(-n)},\ \boldsymbol{G}_{n-1}^{(-n)},\ \ldots,\ \boldsymbol{G}_1^{(-n)},\ \boldsymbol{G}_0^{(-n)}\right\}$ whose elements are obtained inductively by solving Lyapunov-type equations; see (79), the first equation of (80), (81), the first equation of (82), (83) and (87) in Man et al. (2015).

In what follows under assumption (*) we shall apply a perturbation argument to the aforementioned equations in Man et al. (2015) to derive equations for the matrices which approximate $\mathbf{Z}_n(v)$ $(n=1,2,3,\ldots)$ to within terms linear in $\mathring{\boldsymbol{T}}(0)$ and $\mathbb{A}(0)$. For

$$\boldsymbol{K}_0=\mathbf{T}_0^{-1}\mathbf{R}_0^T-i\mathbf{T}_0^{-1}\mathbf{Z}_0, \tag{17}$$

which appears in all the left hand sides of the aforementioned equations in Man et al. (2015), we can write

$$\boldsymbol{K}_0\approx\boldsymbol{K}_0^{\mathrm{Iso}}+\boldsymbol{K}_0^{\mathrm{Ptb}}, \tag{18}$$

where $\boldsymbol{K}_0^{\mathrm{Iso}}$ is of zeroth order in $\mathring{\boldsymbol{T}}(0)$ and $\mathbb{A}(0)$, and $\boldsymbol{K}_0^{\mathrm{Ptb}}$ is of first order in $\mathring{\boldsymbol{T}}(0)$ and $\mathbb{A}(0)$. It then follows from (13) that

$$\boldsymbol{K}_0^{\mathrm{Iso}}=\begin{pmatrix}-ik_{11} & 0 & 0\\ 0 & -ik_{22} & k_{32}\\ 0 & k_{23} & -ik_{33}\end{pmatrix},$$

where

$$k_{11}=\sqrt{\frac{\mu-V}{\mu}},\quad k_{22}=\sqrt{\frac{\lambda+2\mu-V}{\mu}}H,\quad k_{33}=\sqrt{\frac{\mu-V}{\lambda+2\mu}}H,\quad k_{23}=\sqrt{\frac{\lambda+2\mu-V}{\lambda+2\mu}}J,\quad k_{32}=\sqrt{\frac{\mu-V}{\mu}}J,$$
$$H=\frac{\sqrt{\mu(\lambda+2\mu)}+\sqrt{(\mu-V)(\lambda+2\mu-V)}}{\lambda+3\mu-V},\quad J=\frac{\sqrt{(\lambda+2\mu)(\lambda+2\mu-V)}-\sqrt{\mu(\mu-V)}}{\lambda+3\mu-V}.$$

It also follows that

$$\boldsymbol{K}_0^{\mathrm{Ptb}}=\begin{pmatrix}1/\mu & 0 & 0\\ 0 & 1/\mu & 0\\ 0 & 0 & 1/(\lambda+2\mu)\end{pmatrix}\left(-\mathbf{T}_0^{\mathrm{Ptb}}\boldsymbol{K}_0^{\mathrm{Iso}}+\left(\mathbf{R}_0^{\mathrm{Ptb}}\right)^T-i\mathbf{Z}_0^{\mathrm{Ptb}}\right),$$

where $\mathbf{R}_0^{\mathrm{Ptb}}$ and $\mathbf{T}_0^{\mathrm{Ptb}}$ are equal to the matrices $\mathbf{R}_n$ and $\mathbf{T}_n$ in (19) below with $n=0$, $\mathring{T}_{23}(0)=\mathring{T}_{33}(0)=0$, respectively.

Since $\mathbf{Z}_n(\nu)$ $(n=1,2,3,\ldots)$ are related to $\boldsymbol{G}_0^{(-n)}$ by (16), it is sufficient to give equations which determine $\boldsymbol{G}_l^{(-n)}$ $(l=0,1,2,\ldots,n)$ to within terms linear in $\mathbb{A}(0)$ and $\mathring{\boldsymbol{T}}(0)$. Hereafter we use the symbol " $\widetilde{\boldsymbol{G}_l^{(-n)}}$ " to denote a matrix which approximates $\boldsymbol{G}_l^{(-n)}$ up to terms linear in $\mathbb{A}(0)$ and $\mathring{\boldsymbol{T}}(0)$ $(n=1,2,3,\ldots;l=0,1,2,\ldots,n)$.

From (15) it follows that for $n=1,2,3,\ldots$,

$$\mathbf{Q}_n=\frac{1}{n!}\begin{pmatrix}\frac{\partial^n}{\partial x_3^n}(a_{66}+\mathring{T}_{22}-\rho v^2)\Big|_{x_3=0} & \frac{\partial^n}{\partial x_3^n}a_{26}\Big|_{x_3=0} & \frac{\partial^n}{\partial x_3^n}a_{46}\Big|_{x_3=0}\\ \frac{\partial^n}{\partial x_3^n}a_{26}\Big|_{x_3=0} & \frac{\partial^n}{\partial x_3^n}(a_{22}+\mathring{T}_{22}-\rho v^2)\Big|_{x_3=0} & \frac{\partial^n}{\partial x_3^n}a_{24}\Big|_{x_3=0}\\ \frac{\partial^n}{\partial x_3^n}a_{46}\Big|_{x_3=0} & \frac{\partial^n}{\partial x_3^n}a_{24}\Big|_{x_3=0} & \frac{\partial^n}{\partial x_3^n}(a_{44}+\mathring{T}_{22}-\rho v^2)\Big|_{x_3=0}\end{pmatrix},$$

$$\mathbf{R}_n=\frac{1}{n!}\begin{pmatrix}\frac{\partial^n}{\partial x_3^n}(a_{56}+\mathring{T}_{23})\Big|_{x_3=0} & \frac{\partial^n}{\partial x_3^n}a_{46}\Big|_{x_3=0} & \frac{\partial^n}{\partial x_3^n}a_{36}\Big|_{x_3=0}\\ \frac{\partial^n}{\partial x_3^n}a_{25}\Big|_{x_3=0} & \frac{\partial^n}{\partial x_3^n}(a_{24}+\mathring{T}_{23})\Big|_{x_3=0} & \frac{\partial^n}{\partial x_3^n}a_{23}\Big|_{x_3=0}\\ \frac{\partial^n}{\partial x_3^n}a_{45}\Big|_{x_3=0} & \frac{\partial^n}{\partial x_3^n}a_{44}\Big|_{x_3=0} & \frac{\partial^n}{\partial x_3^n}(a_{34}+\mathring{T}_{23})\Big|_{x_3=0}\end{pmatrix}, \tag{19}$$

$$\mathbf{T}_n=\frac{1}{n!}\begin{pmatrix}\frac{\partial^n}{\partial x_3^n}(a_{55}+\mathring{T}_{33})\Big|_{x_3=0} & \frac{\partial^n}{\partial x_3^n}a_{45}\Big|_{x_3=0} & \frac{\partial^n}{\partial x_3^n}a_{35}\Big|_{x_3=0}\\ \frac{\partial^n}{\partial x_3^n}a_{45}\Big|_{x_3=0} & \frac{\partial^n}{\partial x_3^n}(a_{44}+\mathring{T}_{33})\Big|_{x_3=0} & \frac{\partial^n}{\partial x_3^n}a_{34}\Big|_{x_3=0}\\ \frac{\partial^n}{\partial x_3^n}a_{35}\Big|_{x_3=0} & \frac{\partial^n}{\partial x_3^n}a_{34}\Big|_{x_3=0} & \frac{\partial^n}{\partial x_3^n}(a_{33}+\mathring{T}_{33})\Big|_{x_3=0}\end{pmatrix}.$$

Putting $m=1$ in (79) of Man et al. (2015) and taking account of (18) and $-\mathbf{T}_0\mathbf{S}_1\mathbf{T}_0=\mathbf{T}_1$, we observe that $\widetilde{\boldsymbol{G}_1^{(-1)}}$ is obtained as the solution to

$$\left(\boldsymbol{K}_0^{\mathrm{Iso}}+\boldsymbol{K}_0^{\mathrm{Ptb}}\right)^*\widetilde{\boldsymbol{G}_1^{(-1)}}-\widetilde{\boldsymbol{G}_1^{(-1)}}\left(\boldsymbol{K}_0^{\mathrm{Iso}}+\boldsymbol{K}_0^{\mathrm{Ptb}}\right)=\mathbf{Q}_1-\left(\mathbf{R}_1+\mathbf{R}_1^T\right)\left(\boldsymbol{K}_0^{\mathrm{Iso}}+\boldsymbol{K}_0^{\mathrm{Ptb}}\right)+\left(\boldsymbol{K}_0^{\mathrm{Iso}}\right)^*\mathbf{T}_1\boldsymbol{K}_0^{\mathrm{Iso}}+2\mathcal{H}\left(\left(\boldsymbol{K}_0^{\mathrm{Iso}}\right)^*\mathbf{T}_1\boldsymbol{K}_0^{\mathrm{Ptb}}\right), \tag{20}$$

where $\mathbf{M}^*$ denotes the adjoint of the matrix $\mathbf{M}$ (i.e., $\mathbf{M}^*=\overline{\mathbf{M}^{\mathbf{T}}}$) and $\mathcal{H}(\mathbf{M})$ denotes the Hermitian part of $\mathbf{M}$, i.e., $\mathcal{H}(\mathbf{M})=\frac{1}{2}(\mathbf{M}+\mathbf{M}^*)$. Eq. (20) is of Lyapunov type. All the eigenvalues of $\boldsymbol{K}_0$ (17) have negative imaginary parts (cf. Proposition 1 in Section 3 of Man et al. (2015)), which implies under assumption (*) that (20) can be solved for $\widetilde{\boldsymbol{G}_1^{(-1)}}$ uniquely in terms of the right-hand side (cf. Section 8.3 of Gantmacher (1960) or Chapter 12 of Bellman (1997)).

Once we have obtained $\widetilde{\boldsymbol{G}_1^{(-1)}}$, putting $m=1$ in (81) and in the first equation of (80) in Man et al. (2015), we see that $\widetilde{\boldsymbol{G}_0^{(-1)}}$ is obtained as the solution to

$$\left(\boldsymbol{K}_0^{\mathrm{Iso}}+\boldsymbol{K}_0^{\mathrm{Ptb}}\right)^*\widetilde{\boldsymbol{G}_0^{(-1)}}-\widetilde{\boldsymbol{G}_0^{(-1)}}\left(\boldsymbol{K}_0^{\mathrm{Iso}}+\boldsymbol{K}_0^{\mathrm{Ptb}}\right)=i\left(\mathbf{R}_1^T-\widetilde{\boldsymbol{G}_1^{(-1)}}\right). \tag{21}$$

Then, $\mathbf{Z}_1\approx i\widetilde{\boldsymbol{G}_0^{(-1)}}$.

For $m=2,3,4,\ldots$, suppose that we have obtained the sequences of matrices

$$\left\{\widetilde{\boldsymbol{G}_1^{(-1)}},\ \widetilde{\boldsymbol{G}_0^{(-1)}}\right\},\quad\left\{\widetilde{\boldsymbol{G}_2^{(-2)}},\ \widetilde{\boldsymbol{G}_1^{(-2)}},\ \widetilde{\boldsymbol{G}_0^{(-2)}}\right\},\quad\ldots,\quad\left\{\boldsymbol{G}_{m-1}^{(\widetilde{-(m-1)})},\ \boldsymbol{G}_{m-2}^{(\widetilde{-(m-1)})},\ \ldots,\ \boldsymbol{G}_1^{(\widetilde{-(m-1)})},\ \boldsymbol{G}_0^{(\widetilde{-(m-1)})}\right\}. \tag{22}$$

Then the sequence $\{\widetilde{\boldsymbol{G}_m^{(-m)}},\ \widetilde{\boldsymbol{G}_{m-1}^{(-m)}},\ \ldots,\ \widetilde{\boldsymbol{G}_1^{(-m)}},\ \widetilde{\boldsymbol{G}_0^{(-m)}}\}$ is determined as follows: Eqs. (79) and (87) in Man et al. (2015), combined with (18), imply that $\widetilde{\boldsymbol{G}_m^{(-m)}}$ can be obtained as the solution to

$$\left(\boldsymbol{K}_0^{\mathrm{Iso}}+\boldsymbol{K}_0^{\mathrm{Ptb}}\right)^*\widetilde{\boldsymbol{G}_m^{(-m)}}-\widetilde{\boldsymbol{G}_m^{(-m)}}\left(\boldsymbol{K}_0^{\mathrm{Iso}}+\boldsymbol{K}_0^{\mathrm{Ptb}}\right)=\mathbf{Q}_m-\left(\mathbf{R}_m+\mathbf{R}_m^T\right)\left(\boldsymbol{K}_0^{\mathrm{Iso}}+\boldsymbol{K}_0^{\mathrm{Ptb}}\right)-\left(\boldsymbol{K}_0^{\mathrm{Iso}}+\boldsymbol{K}_0^{\mathrm{Ptb}}\right)^*\left(\widetilde{\mathbf{S}_0}\right)^{-1}\widetilde{\mathbf{S}_m}\left(\widetilde{\mathbf{S}_0}\right)^{-1}\left(\boldsymbol{K}_0^{\mathrm{Iso}}+\boldsymbol{K}_0^{\mathrm{Ptb}}\right)-\widetilde{\mathcal{F}_1^m}, \tag{23}$$

where

$$\widetilde{\mathbf{S}_0} = \left(\mathbf{T}_0^{\mathrm{Iso}}\right)^{-1} - \left(\mathbf{T}_0^{\mathrm{Iso}}\right)^{-1}\mathbf{T}_0^{\mathrm{Ptb}}\left(\mathbf{T}_0^{\mathrm{Iso}}\right)^{-1},\quad \widetilde{\mathbf{S}_n} = \sum_{k=1}^{n}(-1)^k \sum_{\substack{l_1+l_2+\cdots+l_k=n \\ 1\le l_1,l_2,\ldots,l_k}} \left(\widetilde{\mathbf{S}_0}\mathbf{T}_{l_1}\right)\left(\widetilde{\mathbf{S}_0}\mathbf{T}_{l_2}\right)\cdots\left(\widetilde{\mathbf{S}_0}\mathbf{T}_{l_k}\right)\widetilde{\mathbf{S}_0}\quad (n=1,2,3,\ldots)$$

approximate $\mathbf{S}_0 = (\mathbf{T}_0)^{-1}$ and $\mathbf{S}_n$ $(n=1,2,3,\ldots)$ up to terms linear in $\mathring{\boldsymbol{T}}(0)$ and $\mathbb{A}(0)$, respectively,

$$\widetilde{\mathcal{F}_1^m} = \sum_{\alpha=1}^{m-1}\left(\widetilde{\boldsymbol{G}_\alpha^{(-\alpha)}}\right)^*\widetilde{\mathbf{S}_0}\,\widetilde{\boldsymbol{G}_{m-\alpha}^{(-(m-\alpha))}} + 2\mathcal{H}\left(\sum_{n=1}^{m-1}\left(\widetilde{\boldsymbol{G}_{m-n}^{(-(m-n))}}\right)^*\widetilde{\mathbf{S}_n}\left(\widetilde{\mathbf{S}_0}\right)^{-1}\left(\boldsymbol{K}_0^{\mathrm{Iso}}+\boldsymbol{K}_0^{\mathrm{Ptb}}\right)\right) + \sum_{n=1}^{m-2}\sum_{\alpha=1}^{m-n-1}\left(\widetilde{\boldsymbol{G}_\alpha^{(-\alpha)}}\right)^*\widetilde{\mathbf{S}_n}\,\widetilde{\boldsymbol{G}_{m-\alpha-n}^{(-(m-\alpha-n))}},$$

and the last term on the right hand side of the preceding equation drops out when $m=2$. Note that $\widetilde{\mathcal{F}_1^m}$ is determined from the entries in (22). Hence we can solve (23) for $\widetilde{\boldsymbol{G}_m^{(-m)}}$ uniquely.

Once we have obtained $\widetilde{\boldsymbol{G}_m^{(-m)}}$, from (81) and the first equation of (80) in Man et al. (2015) we see that $\widetilde{\boldsymbol{G}_{m-1}^{(-m)}}$ can be obtained as the solution to

$$\left(\boldsymbol{K}_0^{\mathrm{Iso}}+\boldsymbol{K}_0^{\mathrm{Ptb}}\right)^*\widetilde{\boldsymbol{G}_{m-1}^{(-m)}} - \widetilde{\boldsymbol{G}_{m-1}^{(-m)}}\left(\boldsymbol{K}_0^{\mathrm{Iso}}+\boldsymbol{K}_0^{\mathrm{Ptb}}\right) = -\widetilde{\mathcal{F}_2^m} + im\left(\mathbf{R}_m^T - \widetilde{\boldsymbol{G}_m^{(-m)}}\right), \tag{24}$$

where

$$\begin{aligned}\widetilde{\mathcal{F}_2^m} = {} & 2\mathcal{H}\left(\left(\widetilde{\boldsymbol{G}_0^{(-1)}}\right)^*\widetilde{\mathbf{S}_0}\,\widetilde{\boldsymbol{G}_{m-1}^{(-(m-1))}} + \sum_{n=1}^{m-1}\left(\widetilde{\boldsymbol{G}_{m-1-n}^{(-(m-n))}}\right)^*\widetilde{\mathbf{S}_n}\left(\widetilde{\mathbf{S}_0}\right)^{-1}\left(\boldsymbol{K}_0^{\mathrm{Iso}}+\boldsymbol{K}_0^{\mathrm{Ptb}}\right)\right) + \sum_{\alpha=1}^{m-2}\sum_{j=\alpha}^{\alpha+1}\left(\widetilde{\boldsymbol{G}_\alpha^{(-j)}}\right)^*\widetilde{\mathbf{S}_0}\,\widetilde{\boldsymbol{G}_{m-1-\alpha}^{(-(m-j))}} \\ & + 2\mathcal{H}\left(\sum_{n=1}^{m-2}\left(\widetilde{\boldsymbol{G}_{m-1-n}^{(-(m-1-n))}}\right)^*\widetilde{\mathbf{S}_n}\,\widetilde{\boldsymbol{G}_0^{(-1)}}\right) + \sum_{n=1}^{m-3}\sum_{\alpha=1}^{m-2-n}\sum_{j=\alpha}^{\alpha+1}\left(\widetilde{\boldsymbol{G}_\alpha^{(-j)}}\right)^*\widetilde{\mathbf{S}_n}\,\widetilde{\boldsymbol{G}_{m-1-\alpha-n}^{(-(m-j-n))}},\end{aligned}$$

and the second and the third terms on the right hand side of the preceding equation drop out when $m=2$ and the last term disappears when $m=2$ and $m=3$. Again, we see that $\widetilde{\mathcal{F}_2^m}$ is determined from the entries in (22). Hence we can solve (24) for $\widetilde{\boldsymbol{G}_{m-1}^{(-m)}}$ uniquely.

For $l=0,1,\ldots,m-2$, suppose that we already know the matrix $\widetilde{\boldsymbol{G}_{l+1}^{(-m)}}$. It then follows from (83) and the first equation of (82) in Man et al. (2015) that $\widetilde{\boldsymbol{G}_l^{(-m)}}$ can be obtained as the solution to

$$\left(\boldsymbol{K}_0^{\mathrm{Iso}}+\boldsymbol{K}_0^{\mathrm{Ptb}}\right)^*\widetilde{\boldsymbol{G}_l^{(-m)}} - \widetilde{\boldsymbol{G}_l^{(-m)}}\left(\boldsymbol{K}_0^{\mathrm{Iso}}+\boldsymbol{K}_0^{\mathrm{Ptb}}\right) = -\widetilde{\mathcal{F}_{3+l}^m} - i(l+1)\,\widetilde{\boldsymbol{G}_{l+1}^{(-m)}}, \tag{25}$$

where

$$\widetilde{\mathcal{F}_{3+l}^m} = \begin{cases} \displaystyle\sum_{j=1}^{m-1}\left(\widetilde{\boldsymbol{G}_0^{(-j)}}\right)^*\widetilde{\mathbf{S}_0}\,\widetilde{\boldsymbol{G}_0^{(-(m-j))}} & \text{for } l=0 \\ 2\mathcal{H}\left(\displaystyle\sum_{j=1}^{m-l}\left(\widetilde{\boldsymbol{G}_0^{(-j)}}\right)^*\widetilde{\mathbf{S}_0}\;\widetilde{\boldsymbol{G}_l^{(-(m-j))}} + \sum_{n=1}^{l}\left(\widetilde{\boldsymbol{G}_{l-n}^{(-(m-n))}}\right)^*\widetilde{\mathbf{S}_n}\left(\widetilde{\mathbf{S}_0}\right)^{-1}\left(\boldsymbol{K}_0^{\mathrm{Iso}}+\boldsymbol{K}_0^{\mathrm{Ptb}}\right)\right) & \\ \quad + \displaystyle\sum_{j=1}^{m-l-1}\left(\widetilde{\boldsymbol{G}_0^{(-j)}}\right)^*\widetilde{\mathbf{S}_l}\;\widetilde{\boldsymbol{G}_0^{(-(m-j-l))}} + \sum_{\alpha=1}^{l-1}\sum_{j=\alpha}^{\alpha+m-l}\left(\widetilde{\boldsymbol{G}_\alpha^{(-j)}}\right)^*\widetilde{\mathbf{S}_0}\;\widetilde{\boldsymbol{G}_{l-\alpha}^{(-(m-j))}} & \\ \quad + 2\mathcal{H}\left(\displaystyle\sum_{n=1}^{l-1}\sum_{j=l-n}^{m-n-1}\left(\widetilde{\boldsymbol{G}_{l-n}^{(-j)}}\right)^*\widetilde{\mathbf{S}_n}\,\widetilde{\boldsymbol{G}_0^{(-(m-j-n))}}\right) + \displaystyle\sum_{n=1}^{l-2}\sum_{\alpha=1}^{l-n-1}\sum_{j=\alpha}^{\alpha+m-l}\left(\widetilde{\boldsymbol{G}_\alpha^{(-j)}}\right)^*\widetilde{\mathbf{S}_n}\,\widetilde{\boldsymbol{G}_{l-\alpha-n}^{(-(m-j-n))}} & \text{for } l\geqslant 1 \end{cases},$$

and the third and the fourth terms on the right hand side of the preceding equation for $l\geqslant 1$ are not there when $l=1$ and the last term drops out when $l=1$ and $l=2$. We see that $\widetilde{\mathcal{F}_{3+l}^m}$ is determined from the entries in (22). Hence we can solve (25) for $\boldsymbol{G}_l^{(-m)}$ uniquely. Then $\mathbf{Z}_m \approx i\,\widetilde{\boldsymbol{G}_0^{(-m)}}$.

Finally, we comment on how to solve (20), (21), (23)–(25). These equations can all be expressed in the form of a Lyapunov-type equation for $\boldsymbol{G}$, namely:

$$\boldsymbol{L}^*\boldsymbol{G} - \boldsymbol{G}\boldsymbol{L} = \boldsymbol{B}, \tag{26}$$

where $\boldsymbol{L} = \boldsymbol{K}_0^{\mathrm{Iso}} + \boldsymbol{K}_0^{\mathrm{Ptb}}$ and $\boldsymbol{B}$ denotes the right hand sides of the respective equations. The three-dimensional matrix equation (26) can be recast into a nine-dimensional linear system. In fact, under the component-wise expressions of the 3×3 matrices

$$\boldsymbol{L} = (l_{ij}),\quad \boldsymbol{G} = (g_{ij}),\quad \boldsymbol{B} = (b_{ij}),$$

(26) is equivalent to

$$\mathcal{L}\boldsymbol{g} = \boldsymbol{b}, \tag{27}$$

where $\mathcal{L}$ is the 9×9 matrix given by

$$\begin{pmatrix}
\overline{l_{11}} - l_{11} & -l_{21} & -l_{31} & \overline{l_{21}} & \overline{l_{31}} & 0 & 0 & 0 & 0 \\
-l_{12} & \overline{l_{11}} - l_{22} & -l_{32} & 0 & 0 & \overline{l_{21}} & 0 & \overline{l_{31}} & 0 \\
-l_{13} & -l_{23} & \overline{l_{11}} - l_{33} & 0 & 0 & 0 & \overline{l_{21}} & 0 & \overline{l_{31}} \\
\overline{l_{12}} & 0 & 0 & \overline{l_{22}} - l_{11} & \overline{l_{32}} & -l_{21} & -l_{31} & 0 & 0 \\
\overline{l_{13}} & 0 & 0 & \overline{l_{23}} & \overline{l_{33}} - l_{11} & 0 & 0 & -l_{21} & -l_{31} \\
0 & \overline{l_{12}} & 0 & -l_{12} & 0 & \overline{l_{22}} - l_{22} & -l_{32} & \overline{l_{32}} & 0 \\
0 & 0 & \overline{l_{12}} & -l_{13} & 0 & -l_{23} & \overline{l_{22}} - l_{33} & 0 & \overline{l_{32}} \\
0 & \overline{l_{13}} & 0 & 0 & -l_{12} & \overline{l_{23}} & 0 & \overline{l_{33}} - l_{22} & -l_{32} \\
0 & 0 & \overline{l_{13}} & 0 & -l_{13} & 0 & \overline{l_{23}} & -l_{23} & \overline{l_{33}} - l_{33}
\end{pmatrix},$$

and $\boldsymbol{g}$ and $\boldsymbol{b}$ are nine-dimensional column vectors defined by

$$\boldsymbol{g} = (g_{11}\ g_{12}\ g_{13}\ g_{21}\ g_{31}\ g_{22}\ g_{23}\ g_{32}\ g_{33})^T, \quad \boldsymbol{b} = (b_{11}\ b_{12}\ b_{13}\ b_{21}\ b_{31}\ b_{22}\ b_{23}\ b_{32}\ b_{33})^T.$$

Later in the numerical implementations we shall solve (20) and (21), and the series of (23)–(25) for $m = 2$ and $m = 3$ by appealing to the reduction of them to a nine-dimensional linear system of the form (27) in order to compute the first several terms of asymptotic expansion (9).

Remark 4.1. For a vertically-inhomogeneous anisotropic elastic half-space, several papers have been published on the surface impedance matrix that pertains to surface waves propagating along its surface (cf. Remarks 1 and 2 in Section 5 of Man et al. (2015)). Recently, using the properties of this matrix, Katchalov (2012) proved the existence and the uniqueness of the Rayleigh wave for weakly anisotropic media.

5. Asymptotic formula for phase velocity of Rayleigh waves

We apply the implicit function theorem to the asymptotic representation (10) of the secular equation to obtain the asymptotic formula (7) of v_R for a large wave number k. This procedure is a simple routine and is outlined in Section 6 of Man et al. (2015). Here we note that the first term of (7), namely v_0, solves $\det \mathbf{Z}_0(v) = 0$, i.e., v_0 is the phase velocity of Rayleigh waves propagating along the surface of the comparative homogeneous elastic half-space $x_3 \leqslant 0$ whose incremental elasticity tensor has the form (11), whose initial stress $\mathring{\boldsymbol{T}}(0)$ has the components $\mathring{T}_{i3} = 0$ for $i = 1, 2, 3$, and whose density is equal to $\rho(0)$. By (12), v_0 is written as

$$v_0 \approx v_0^{\mathrm{Iso}} + v_0^{\mathrm{Ptb}}, \tag{28}$$

where v_0^{Iso} and v_0^{Ptb} are of zeroth and first order in $\mathring{\boldsymbol{T}}(0)$ and $\mathbb{A}(0)$, respectively. The term v_0^{Iso} is the velocity of Rayleigh waves in the isotropic medium defined by $\mathbb{L} = \mathbb{C}^{\mathrm{Iso}}$, $\mathbb{A}(0) = \mathbf{0}$, and $\mathring{\boldsymbol{T}}(0) = \mathbf{0}$. A formula for v_0^{Ptb}, with each coefficient of $\mathring{\boldsymbol{T}}(0)$ and $\mathbb{A}(0)$ written explicitly in terms of λ and μ of $\mathbb{C}^{\mathrm{Iso}}$, is given in formula (12) of Tanuma and Man (2006).

To obtain v_i $(i = 1, 2, 3, \ldots)$ in the lower-order terms of (7), we can use the procedure in Section 6 of Man et al. (2015) with v_0 there replaced by $v_0^{\mathrm{Iso}} + v_0^{\mathrm{Ptb}}$.

Finally, let us comment on how each component of $\mathring{\boldsymbol{T}}$ and $\mathbb{A}$ under their respective most general form would affect each term of v_i $(i = 1, 2, 3, \ldots)$. We can deduce the following two assertions from (10), Proposition 3.2, (19) and Lyapunov-type equations (20), (21) and (23)–(25). Recall that the Rayleigh waves in question propagate in the direction of the 2-axis along the surface of the vertically-inhomogeneous, prestressed, anisotropic elastic half-space $x_3 \leqslant 0$, where the constitutive equation is expressed by (1), the incremental elasticity tensor has the form (2), and the mass density is given by $\rho(x_3)$.

1. To obtain the terms in (7) up to those of v_n, it suffices to know $\lambda, \mu, \mathring{\boldsymbol{T}}(0), \mathbb{A}(0), \rho(0)$ and the x_3-derivatives of $\mathbb{A}(x_3), \mathring{\boldsymbol{T}}(x_3), \rho(x_3)$ at $x_3 = 0$ up to those of order n.
2. None of the components of $\mathbb{A}(x_3)$ which have the subscript "1" in the Voigt notation and none of the components of $\mathring{\boldsymbol{T}}(x_3)$ which have the subscript "1" can affect the dispersion of Rayleigh waves.

6. An illustrative example

Among engineering material systems covered by the theory developed in this paper are metal structural parts surface-treated by low plasticity burnishing (LPB), which leaves a mirror-smooth surface finish and creates a thin layer of compressive residual stress that improves the fatigue life of the parts so treated. The situation at issue is similar to those of many applications that involve elastic waves in structural metals (see Man (1999) and the references therein), where the perturbative part $\mathbb{A}$ in the splitting (2) of the incremental elasticity tensor $\mathbb{L}$ is originated from the presence of crystallographic texture and of the prestress. Moreover, the shifts in phase velocities of elastic waves caused by texture and initial stress (with the latter bounded by the yield surface) are typically within 2% of their values for the corresponding isotropic medium with $\mathbb{L} = \mathbb{C}^{\mathrm{Iso}}$, which suggests that linearization assumption (*) would be adequate. As we shall illustrate in Table 1 below, the example that we shall study in this section is no different.

One problem of considerable engineering interest concerns the possibility of using Rayleigh waves to monitor the retention of the protective prestress $\overset{\circ}{\boldsymbol{T}}$ during the lifetime of a structural component. We shall study this inverse problem in another paper. Our solution of the inverse problem, however, is based on what we have done above on the direct problem to determine dispersion curves for Rayleigh waves propagating in various directions when the material parameters, texture coefficients, and initial stresses are given. In this section, we illustrate our solution of this direct problem by a concrete example.

A 10 cm × 10 cm × 2 cm sample was cut from an AA 7075-T651 aluminum plate. One face of the sample was surface treated with low plasticity burnishing, which introduced in the sample depth-dependent compressive stresses to a depth of about 1 mm from the treated surface (cf. Moreau & Man (2006) for more details on sample preparation). Henceforth we fix a spatial coordinate system $OXYZ$ and model the prestressed sample as a half space that occupies the region $x_3 \leqslant 0$, while the 1- and 2-axis are chosen arbitrarily. By the "depth" of a point in the material half-space is meant the value of $-x_3$ (in mm), where x_3 is the 3-coordinate of the given point. We consider only Rayleigh waves propagating in the direction of the 2-axis. X-ray diffraction measurements indicated that there were three distinguished mutually-orthogonal directions for material points at the LPB-treated surface of the sample, namely the 3-direction (normal to the free surface), the direction of LPB-rolling (which apparently was the same as the original rolling direction of the manufacturing process), and the direction transverse to the two. We define another Cartesian coordinate system $OX'Y'Z'$ which has the $1'$-, $2'$-, and $3'$-axis agree with the aforementioned rolling, transverse, and normal direction (i.e., the 3-direction) of the sample, respectively. We call $OX'Y'Z'$ the material coordinate system, because it is attached to the sample. Let θ be the angle of rotation about the 3-axis that will bring the 2-axis to the $2'$-axis. Different propagation directions in the sample are obtained by rotating the material half-space about the 3-axis, i.e., by varying θ. Henceforth we call θ the propagation direction of the Rayleigh wave (relative to the $2'$-direction of the material half-space).

The surface and near-surface crystallographic texture of the sample at the LPB-treated face were measured by X-ray diffraction up to a depth of 0.225 mm. The texture was found to be essentially constant with depth and was orthorhombic with respect to the $O'X'Y'Z'$ coordinate system. The values of those texture coefficients relevant to this study, namely $W'_{400}, W'_{420}, W'_{440}, W'_{600}, W'_{620}, W'_{640}$ and W'_{660}, are given in Appendix B. Regrettably, for the 7075-T651 sample, texture measurement was not made at depths that exceed 0.225 mm, as the material within a surface layer of about 1 mm thick would be relevant to the present study. For the present purpose of working out an illustrative example, we will simply take the crystallographic texture to be constant at all depths in our model of the sample.

The depth-dependent prestress, assumed to be of the form

$$\overset{\circ}{\boldsymbol{T}}(x_3) = \begin{pmatrix} \overset{\circ}{T}_{11}(x_3) & \overset{\circ}{T}_{12}(x_3) & 0 \\ \overset{\circ}{T}_{12}(x_3) & \overset{\circ}{T}_{22}(x_3) & 0 \\ 0 & 0 & 0 \end{pmatrix} \tag{29}$$

under the $OXYZ$ coordinate system, was measured by X-ray diffraction (and supplemented by information gathered from hole-drilling) up to a depth of 1.25 mm from the treated surface. Let $\mathbf{e}_1(x_3)$ and $\mathbf{e}_2(x_3)$ be the principal directions of the stress that are perpendicular to the 3-axis, and $\sigma_1(x_3)$ and $\sigma_2(x_3)$ be the corresponding principal stresses. Let $\zeta(x_3)$ be the angle between $\mathbf{e}_2(x_3)$ and the $2'$-axis. Then $\varphi(x_3) = \theta + \zeta(x_3)$ is the angle of rotation about the 3-axis that will bring the direction of the 2-axis to $\mathbf{e}_2(x_3)$; see Fig. 1. It follows that $\overset{\circ}{T}_{ij}(x_3)$ in (29) can be written as

$$\overset{\circ}{T}_{11} = \overset{\circ}{T}_m - \overset{\circ}{T}_d \cos 2\varphi, \quad \overset{\circ}{T}_{22} = \overset{\circ}{T}_m + \overset{\circ}{T}_d \cos 2\varphi, \quad \overset{\circ}{T}_{12} = -\overset{\circ}{T}_d \sin 2\varphi, \tag{30}$$

where

$$\overset{\circ}{T}_m := \frac{\sigma_1 + \sigma_2}{2}, \quad \overset{\circ}{T}_d := \frac{\sigma_2 - \sigma_1}{2}. \tag{31}$$

The measured data-points of the principal stresses σ_1 and σ_2 are shown in Fig. 2, where adjacent data-points are joined by straight-line segments. The top (red) curve and the bottom (blue) curve give the principal stresses σ_1 and σ_2, respectively. In

Table 1
Zeroth-order velocity v_0 (in m/s) for Rayleigh waves with different propagation directions θ in sample prestressed half-space with three different textures. For comparison, $v_0^{\text{iso}} = 2891.4$ m/s.

θ (degree)	0°	45°	90°	135°
Texture (I)	2882.7	2873.1	2873.2	2877.7
Texture (II)	2867.3	2874.2	2881.4	2878.3
No texture	2876.4	2867.8	2863.8	2872.4

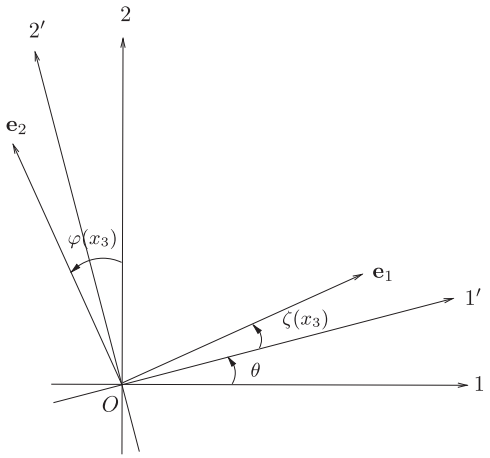

Fig. 1. Spatial coordinate system, material coordinate system, and principal-stress directions.

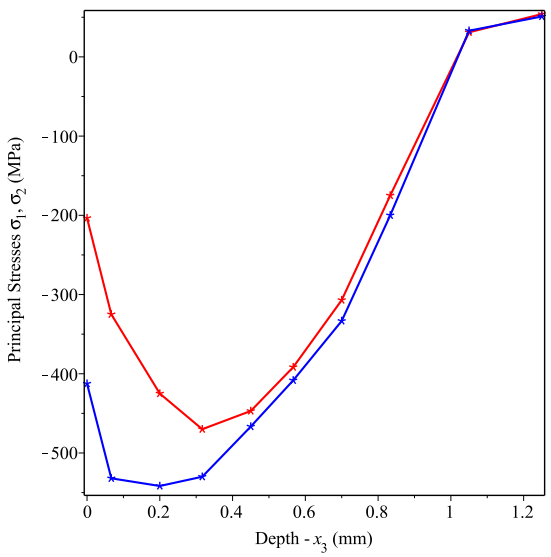

Fig. 2. Depth profiles of principal stresses σ_1 (top curve) and σ_2 (bottom curve).

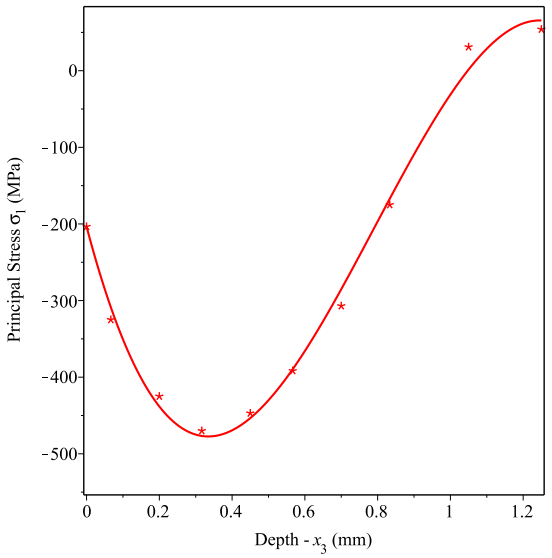

Fig. 3. Graph of cubic polynomial that fits the data points of principal stress σ_1.

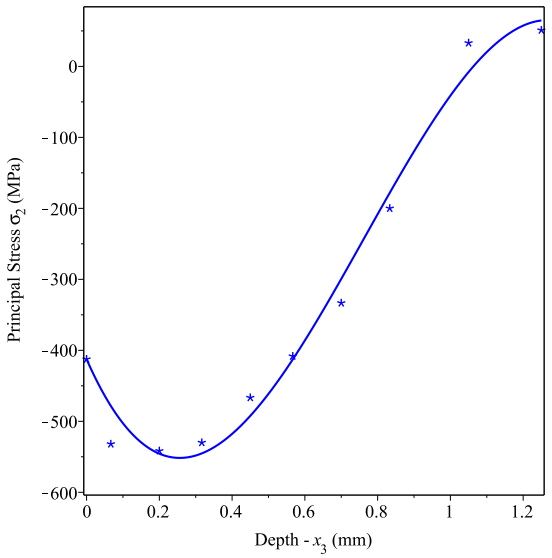

Fig. 4. Graph of cubic polynomial that fits the data points of principal stress σ_2.

our model we fit the data points with cubic polynomials. The cubic fitting curves for the principal stresses σ_1 and σ_2 are shown in Figs. 3 and 4, respectively. The corresponding equations of the principal stresses are given by

$$\sigma_1(x_3) = 1.4387 \times 10^3 x_3^3 + 3.4090 \times 10^3 x_3^2 + 1.7981 \times 10^3 x_3 - 2.035 \times 10^2, \tag{32}$$

$$\sigma_2(x_3) = 1.1943 \times 10^3 x_3^3 + 2.7291 \times 10^3 x_3^2 + 1.1636 \times 10^3 x_3 - 4.125 \times 10^2, \tag{33}$$

where σ_1, σ_2 are in MPa and x_3 is in mm.

In the stress measurements it was found that $\zeta(x_3) \approx 10^\circ$ for $0 \geqslant x_3 \geqslant -0.5$ mm. As shown in Fig. 2, $\sigma_1(x_3) \approx \sigma_2(x_3)$ for $x_3 \leqslant -0.5$ mm. Hence we may take $\zeta(x_3) \approx 10^\circ$ for $x_3 \leqslant -0.5$ mm, as $\zeta(x_3)$ is, to within experimental error, arbitrary there. In our example, we will simply put $\zeta(x_3) = 10^\circ$ for all $x_3 \leqslant 0$ in our model of the sample. Later in our computations, we shall have to make use of the components $\overset{\circ}{T}_{ij}(x_3)$ of the prestress under the *OXYZ* coordinate system. The non-trivial components

$\mathring{T}_{ij}(x_3)$ that pertain to (32) and (33) for the principal stresses, $\zeta(x_3) = 10^\circ$, and various propagation direction θ can be obtained from (30) and (31), where $\varphi = \theta + \zeta(x_3)$.

We treat the material points of the prestressed 7075-T651 aluminum sample as weakly-textured orthorhombic aggregates of cubic crystallites and, in our model, adopt what follows as their constitutive equation under the $OX'Y'Z'$ material coordinate system (cf. Man (1999), Tanuma & Man (2002)):

$$\begin{aligned}\boldsymbol{S} &= \mathring{\boldsymbol{T}} + \boldsymbol{H}\mathring{\boldsymbol{T}} + \mathbb{L}[\boldsymbol{E}] = \mathring{\boldsymbol{T}} + \boldsymbol{H}\mathring{\boldsymbol{T}} + \mathbb{C}^{\mathrm{Iso}}[\boldsymbol{E}] + \mathbb{A}[\boldsymbol{E}] \\ &= \mathring{\boldsymbol{T}} + \boldsymbol{H}\mathring{\boldsymbol{T}} + \lambda(\mathrm{tr}\boldsymbol{E})\mathbf{I} + 2\mu\boldsymbol{E} + \alpha\boldsymbol{\Phi}(W'_{400}, W'_{420}, W'_{440})[\boldsymbol{E}] + \beta_1(\mathrm{tr}\mathring{\boldsymbol{T}})(\mathrm{tr}\boldsymbol{E})\mathbf{I} + \beta_2(\mathrm{tr}\mathring{\boldsymbol{T}})\boldsymbol{E} + \beta_3((\mathrm{tr}\boldsymbol{E})\mathring{\boldsymbol{T}} + \mathrm{tr}(\boldsymbol{E}\mathring{\boldsymbol{T}})\mathbf{I}) \\ &\quad + \beta_4(\boldsymbol{E}\mathring{\boldsymbol{T}} + \mathring{\boldsymbol{T}}\boldsymbol{E}) + \sum_{i=1}^{4} b_i \boldsymbol{\Psi}^{(i)}(W'_{400}, W'_{420}, W'_{440})[\mathring{\boldsymbol{T}}, \boldsymbol{E}] + a\boldsymbol{\Theta}(W'_{600}, W'_{620}, W'_{640}, W'_{660})[\mathring{\boldsymbol{T}}, \boldsymbol{E}]. \end{aligned} \tag{34}$$

Here $\boldsymbol{\Phi}$ is a fourth-order tensor and $\boldsymbol{\Psi}^{(i)}$ $(i = 1, \ldots, 4)$ are sixth-order tensors defined in terms of the texture coefficients $W'_{400}, W'_{420}, W'_{440}$, and $\boldsymbol{\Theta}$ a sixth-order tensor defined in terms of $W'_{600}, W'_{620}, W'_{640}$ and W'_{660}. The components of these tensors in the $OXYZ$ coordinate system are given explicitly in Appendix B, and so are the values of the 12 material parameters $\lambda, \mu, \alpha, \beta_i$ $(i = 1, \ldots, 4)$, b_j $(j = 1, \ldots, 4)$, and a adopted for the 7075-T651 aluminum sample in our example.

Let ρ_0 be the density of the aluminum alloy in question when it is stress free. The presence of vertically-inhomogeneous residual stress $\mathring{\boldsymbol{T}}(x_3)$ will change the density of the material point from ρ_0 to $\rho(x_3)$, which is related to ρ_0 and $\mathring{\boldsymbol{T}}(x_3)$ by the formula

$$\rho(x_3) = \rho_0(1 - \mathrm{tr}\boldsymbol{E}), \quad \text{where } \boldsymbol{E} = (\mathbb{C}^{\mathrm{Iso}} + \alpha\boldsymbol{\Phi})^{-1}[\mathring{\boldsymbol{T}}].$$

In our example we take $\rho_0 = 2.81 \times 10^3$ kg/m^3, which is the (nominal) density of AA7075 alloy as computed from those of its alloying elements and their concentrations (Aluminum Standards and Data 2000 (2000), pp. 2–14).

In this paper we want to examine also how the texture would affect the dispersion relations. Hence, for comparison purposes, we consider in addition two hypothetical but possible scenarios in the texture of the 7075-T651 sample to yield three cases as follows:

- The sample has its actual texture, the relevant coefficients of which are given in Appendix B. We call this case Texture (I).
- The texture of the sample has coefficients

$W'_{400} = 0.00159, W'_{420} = -0.00368, W'_{440} = 0.00175, W'_{600} = -0.00529, W'_{620} = 0.00348, W'_{640} = -0.00299,$ and $W'_{660} = 0.00197$.

These coefficients are those that pertain to the surface texture of a 6061-T6 aluminum alloy plate (Man, Lu, & Li, 1999). We refer to this case as Texture (II).

- The 7075-T651 sample has no texture, i.e., $W'_{lm0} = 0$.

From (7) and (28), the dispersion relation can be written in the lower-order terms of the asymptotic expansion as

$$v_R \approx v_0 + v_1\varepsilon + v_2\varepsilon^2 + v_3\varepsilon^3 = v_0^{\mathrm{Iso}} + v_0^{\mathrm{Ptb}} + v_1\varepsilon + v_2\varepsilon^2 + v_3\varepsilon^3, \tag{35}$$

where $\varepsilon = k^{-1}$ and k denotes the wave number. In (35), $v_0 = v_0^{\mathrm{Iso}} + v_0^{\mathrm{Ptb}}$ is the zeroth-order term. As shown by Tanuma and Man (2002), v_0 can be estimated by the formula

$$\begin{aligned} v_0 &= v_0^{\mathrm{Iso}} - \frac{1}{2\rho(0)v_0^{\mathrm{Iso}}} \\ &\quad \times \Big(A_0 + A_2\cos 2\theta + A_4\cos 4\theta + (B_0 + B_2\cos 2\theta + B_4\cos 4\theta)\mathring{T}_m(0) \\ &\quad + (C_0 + C_2\cos 2\theta + C_4\cos 4\theta + C_6\cos 6\theta)\mathring{T}_d(0)\cos 2(\theta + \zeta(0)) \\ &\quad + (D_2\sin 2\theta + D_4\sin 4\theta + D_6\sin 6\theta)\mathring{T}_d(0)\sin 2(\theta + \zeta(0)) \Big); \end{aligned} \tag{36}$$

here v_0^{Iso} is the phase velocity of Rayleigh waves in the isotropic base material; $\rho(0), \mathring{T}_m(0), \mathring{T}_d(0)$, and $\zeta(0)$ are the values of the density ρ, stress parameters $\mathring{T}_m, \mathring{T}_d$, and ζ at the free surface $x_3 = 0$, respectively. Explicit formulas that relate the parameters A_i $(i = 0, 2, 4)$, B_i $(i = 0, 2, 4)$, C_i $(i = 0, 2, 4, 6)$, and D_i $(i = 2, 4, 6)$ to material parameters and texture coefficients are given in Tanuma and Man (2002).

Appealing to (31), and using $\zeta(0) = 10^\circ$ and the values of $\sigma_1(0)$ and $\sigma_2(0)$ given in (32) and (33), respectively, we compute the velocities v_0 of the sample in question for the aforementioned three cases of texture by formula (36) for $\theta = 0^\circ, 45^\circ, 90^\circ$, and 135°. The results are shown in Table 1.

To compute v_i $(i = 1, 2, 3)$, we start from the following truncated form of the asymptotic expansion (9) of the surface impedance $\mathbf{Z}$:

$$\mathbf{Z} = \mathbf{Z}_0^{\mathrm{Iso}} + \mathbf{Z}_0^{\mathrm{Ptb}} + \mathbf{Z}_1\,\varepsilon + \mathbf{Z}_2\,\varepsilon^2 + \mathbf{Z}_3\,\varepsilon^3,$$

where $\mathbf{Z}_0^{\mathrm{Iso}}$ is the surface impedance matrix of the homogeneous isotropic base material with $\mathbb{L} = \mathbb{C}^{\mathrm{Iso}}, \mathbb{A} = \mathbf{O}, \mathring{\boldsymbol{T}} = \mathbf{0}$ and $\rho = \rho(0)$, $\mathbf{Z}_0^{\mathrm{Ptb}}$ is determined by (12), and $\varepsilon = k^{-1}$. We set the approximate secular equation as

$$R(v, \varepsilon) = \det\left[\mathbf{Z}_0^{\mathrm{Iso}} + \mathbf{Z}_0^{\mathrm{Ptb}} + \mathbf{Z}_1\,\varepsilon + \mathbf{Z}_2\,\varepsilon^2 + \mathbf{Z}_3\,\varepsilon^3\right] = 0. \tag{37}$$

By the implicit functions theorem, we obtain from (37) the formulas

$$v_1 = -\frac{N_1}{D}, \quad v_2 = -\frac{N_2}{2D}, \quad v_3 = -\frac{N_3}{6D}, \tag{38}$$

where

$$D = \left.\frac{\partial R}{\partial v}\right|_{v=v_0,\varepsilon=0}, \quad N_1 = \left.\frac{\partial R}{\partial \varepsilon}\right|_{v=v_0,\varepsilon=0}, \quad N_2 = \left.\frac{\partial^2 R}{\partial \varepsilon^2}\right|_{v=v_0,\varepsilon=0} + 2\,v_1 \left.\frac{\partial^2 R}{\partial \varepsilon \partial v}\right|_{v=v_0,\varepsilon=0} + (v_1)^2 \left.\frac{\partial^2 R}{\partial v^2}\right|_{v=v_0,\varepsilon=0},$$

$$N_3 = \left.\frac{\partial^3 R}{\partial \varepsilon^3}\right|_{v=v_0,\varepsilon=0} + 3\,v_1 \left.\frac{\partial^3 R}{\partial \varepsilon^2 \partial v}\right|_{v=v_0,\varepsilon=0} + 3(v_1)^2 \left.\frac{\partial^3 R}{\partial \varepsilon \partial v^2}\right|_{v=v_0,\varepsilon=0} + (v_1)^3 \left.\frac{\partial^3 R}{\partial v^3}\right|_{v=v_0,\varepsilon=0} + 6\,v_2 \left.\frac{\partial^2 R}{\partial \varepsilon \partial v}\right|_{v=v_0,\varepsilon=0} + 6\,v_1 v_2 \left.\frac{\partial^2 R}{\partial v^2}\right|_{v=v_0,\varepsilon=0},$$

and v_0 is estimated by using (36) above.

By (37) and (38) we take the following steps to obtain v_1, v_2, and v_3 in the dispersion relation (35):

Step 1 Determine $\mathbf{Z}_0^{\mathrm{Iso}}$ and $\mathbf{Z}_0^{\mathrm{Ptb}}$ by using the well-known formula reproduced in Proposition 3.1 and the formulas given in Proposition 3.2 and Appendix A, respectively.

Step 2 Determine $\mathbf{Z}_1$ by the formula $\mathbf{Z}_1 = i\widetilde{\boldsymbol{G}_0^{(-1)}}$, where $\widetilde{\boldsymbol{G}_0^{(-1)}}$ is calculated inductively by solving the Lyapunov-type equations (20) and (21).

Step 3 Determine $\mathbf{Z}_2$ by the formula $\mathbf{Z}_2 = i\widetilde{\boldsymbol{G}_0^{(-2)}}$, where $\widetilde{\boldsymbol{G}_0^{(-2)}}$ is obtained inductively by solving Lyapunov-type equations as follows: Solve for $\widetilde{\boldsymbol{G}_2^{(-2)}}$ and $\widetilde{\boldsymbol{G}_1^{(-2)}}$ from (23) and (24) by setting $m = 2$, respectively. Then solve for $\widetilde{\boldsymbol{G}_0^{(-2)}}$ from (25) by setting $m = 2$ and $l = 0$.

Step 4 Determine $\mathbf{Z}_3$ by the formula $\mathbf{Z}_3 = i\widetilde{\boldsymbol{G}_0^{(-3)}}$, where $\widetilde{\boldsymbol{G}_0^{(-3)}}$ is computed inductively by solving Lyapunov-type equations as follows: First solve for $\widetilde{\boldsymbol{G}_3^{(-3)}}$ and $\widetilde{\boldsymbol{G}_2^{(-3)}}$ from (23) and (24) by setting $m = 3$, respectively. Then solve for $\widetilde{\boldsymbol{G}_1^{(-3)}}$ from (25) by setting $m = 3$ and $l = 1$. Finally solve for $\widetilde{\boldsymbol{G}_0^{(-3)}}$ from (25) by setting $m = 3$ and $l = 0$.

Step 5 Compute v_1, v_2 and v_3 from (38).

Step 6 Find the dispersion relation. In practice the limit in accuracy of measurement of v_R is about 0.1%. Hence for the truncated dispersion relation (35), the approximation in replacing v_R by v_0 in the formula $\varepsilon = v_R/(2\pi f)$ will be acceptable if $v_R - v_0$ and the correction terms $v_1/k, v_2/k^2, v_3/k^3$ are all within 1% of v_0. Substitution of $\varepsilon \approx v_0/(2\pi f)$ in the approximate formula (35) for the phase velocity v_R of the Rayleigh waves leads to the dispersion relation between v_R and the frequency f that we seek. See Remark 6.2 for further discussions.

Remark 6.1. We use MAPLE to carry out the above steps. In the program we apply the central finite difference with a fourth-order accuracy to approximate the derivatives with respect to v. The formulas of the finite difference for the first, second and third derivatives are given by

$$\frac{\partial g}{\partial v} = \frac{g(v-2h) - 8g(v-h) + 8g(v+h) - g(v+2h)}{12h} + O(h^4),$$

$$\frac{\partial^2 g}{\partial v^2} = \frac{-g(v-2h) + 16g(v-h) - 30g(v) + 16g(v+h) - g(v+2h)}{12h^2} + O(h^4),$$

$$\frac{\partial^3 g}{\partial v^3} = \frac{g(v-3h) - 8g(v-2h) + 13g(v-h) - 13g(v+h) + 8g(v+2h) - g(v+3h)}{8h^3} + O(h^4).$$

Here g is a given function of v and the step size h is taken to be 0.5 m/s.

The computation results are shown below. For each of the specified propagation directions, the dispersion relations between Rayleigh-wave velocity v_R (in m/s) and frequency f (in Hz) for the sample half-space endowed with the specified prestress and three different textures are as follows:

Case 1 $\theta = 0^\circ$

$$v_R = 2882.7 - \frac{4.248\times 10^7}{\pi f} - \frac{5.224\times 10^{14}}{\pi^2 f^2} + \frac{4.757\times 10^{21}}{\pi^3 f^3} \quad \text{for Texture (I);} \tag{39}$$

$$v_R = 2867.3 - \frac{4.437\times 10^7}{\pi f} - \frac{4.952\times 10^{14}}{\pi^2 f^2} + \frac{4.605\times 10^{21}}{\pi^3 f^3} \quad \text{for Texture (II);} \tag{40}$$

$$v_R = 2876.4 - \frac{2.319\times 10^7}{\pi f} - \frac{7.029\times 10^{14}}{\pi^2 f^2} + \frac{5.432\times 10^{21}}{\pi^3 f^3} \quad \text{for no texture.} \tag{41}$$

The corresponding dispersion curves are shown in Fig. 5.

Case 2 $\theta = 45^\circ$

$$v_R = 2873.1 + \frac{1.879\times 10^8}{\pi f} - \frac{2.586\times 10^{15}}{\pi^2 f^2} + \frac{1.748\times 10^{22}}{\pi^3 f^3} \quad \text{for Texture (I);} \tag{42}$$

$$v_R = 2874.2 + \frac{1.849\times 10^8}{\pi f} - \frac{2.591\times 10^{15}}{\pi^2 f^2} + \frac{1.763\times 10^{22}}{\pi^3 f^3} \quad \text{for Texture (II);} \tag{43}$$

$$v_R = 2867.8 + \frac{8.946\times 10^7}{\pi f} - \frac{1.561\times 10^{15}}{\pi^2 f^2} + \frac{1.035\times 10^{22}}{\pi^3 f^3} \quad \text{for no texture.} \tag{44}$$

The corresponding dispersion curves are shown in Fig. 6.

Case 3 $\theta = 90^\circ$

$$v_R = 2873.2 + \frac{3.154\times 10^8}{\pi f} - \frac{3.714\times 10^{15}}{\pi^2 f^2} + \frac{2.619\times 10^{22}}{\pi^3 f^3} \quad \text{for Texture (I);} \tag{45}$$

$$v_R = 2881.4 + \frac{3.118\times 10^8}{\pi f} - \frac{3.681\times 10^{15}}{\pi^2 f^2} + \frac{2.500\times 10^{22}}{\pi^3 f^3} \quad \text{for Texture (II);} \tag{46}$$

$$v_R = 2863.8 + \frac{1.408\times 10^8}{\pi f} - \frac{1.920\times 10^{15}}{\pi^2 f^2} + \frac{1.172\times 10^{22}}{\pi^3 f^3} \quad \text{for no texture.} \tag{47}$$

The corresponding dispersion curves are shown in Fig. 7.

Case 4 $\theta = 135^\circ$

$$v_R = 2877.7 + \frac{1.239\times 10^8}{\pi f} - \frac{2.093\times 10^{15}}{\pi^2 f^2} + \frac{1.414\times 10^{22}}{\pi^3 f^3} \quad \text{for Texture (I);} \tag{48}$$

$$v_R = 2878.3 + \frac{1.198\times 10^8}{\pi f} - \frac{2.072\times 10^{15}}{\pi^2 f^2} + \frac{1.384\times 10^{22}}{\pi^3 f^3} \quad \text{for Texture (II);} \tag{49}$$

$$v_R = 2872.4 + \frac{2.982\times 10^7}{\pi f} - \frac{1.120\times 10^{15}}{\pi^2 f^2} + \frac{8.103\times 10^{21}}{\pi^3 f^3} \quad \text{for no texture.} \tag{50}$$

The corresponding dispersion curves are shown in Fig. 8.

Remark 6.2. Dispersion relations (39)–(50) are third-order high-frequency asymptotic formulas. Moreover, in obtaining these dispersion relations, we have replaced v_R by v_0 in the formula $\varepsilon := 1/k = v/(2\pi f)$; cf. the discussion under Step 6 just before Remark 6.1. Table 2 displays the values of the first-, second-, and third-order terms in dispersion relation (45), which pertains to Rayleigh waves propagating at $\theta = 90^\circ$ along the treated surface of the 7075-T651 sample. This example is singled out for illustration, partly because it concerns the real-world sample of our primary interest, and partly because it shows the largest dispersion among the cases considered. Note that for $f = 1$ MHz and 2 MHz, we have

$$|v_1|/k \ll |v_2|/k^2 \ll |v_3|/k^3,$$

which suggests that these frequencies are too low for the high-frequency asymptotic formula (45) to be applicable; moreover, the magnitudes of the correction terms in question render the approximation of replacing v_R by v_0 in the formula $\varepsilon = v/(2\pi f)$ problematic. In fact, a glance at Eqs. (39)–(50) reveals that both $|v_2|/(k|v_1|)$ and $|v_3|/(k|v_2|)$ are of the order of $10^7/(\pi f)$, which suggests that these dispersion relations would be applicable for $f \geqslant 5$ or 6 MHz. In practical applications of the dispersion relations delivered by the method presented above, e.g., in using them in nondestructive evaluation of stress, it will be of paramount importance to determine the window of frequencies for which the high-frequency asymptotic

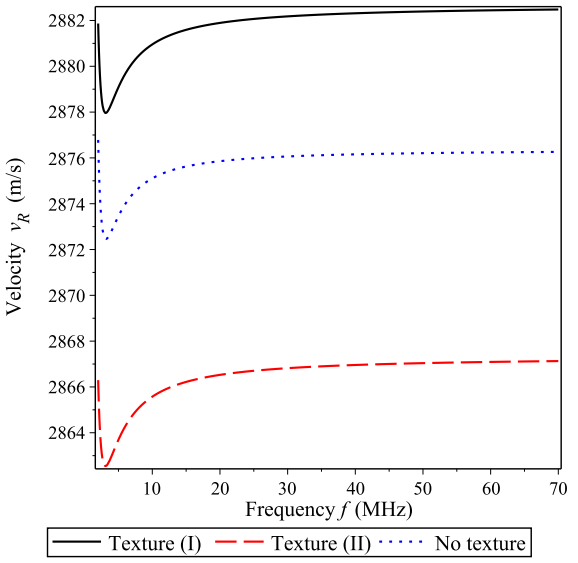

Fig. 5. Dispersion curves for propagation direction $\theta = 0^\circ$.

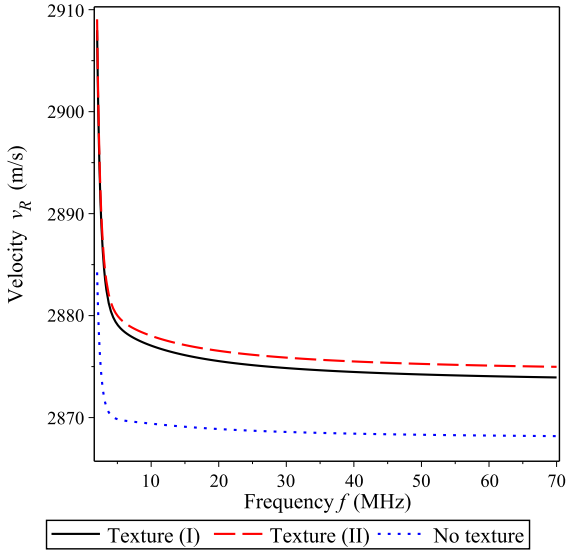

Fig. 6. Dispersion curves for propagation direction $\theta = 45^\circ$.

formulas would be applicable, a task that can be achieved by comparing some of the predicted dispersion relations with the corresponding experimentally-determined dispersion curves.

Remark 6.3. The frequency window within which an nth order dispersion relation is applicable will depend on the order n. In this section, all dispersion relations are computed to the third order. We could push our computations to the fourth order if desired. In fact, that should be pursued in applications where extending the lower end of the frequency window, say to include $f = 4$ MHz as an applicable frequency, is beneficial.

Remark 6.4. In the example above, the texture is assumed to be homogeneous in all three instances considered and the vertical inhomogeneity of the half space is due to that of the principal stresses alone. Even so, Figs. 5–8 show that dispersion is influenced by homogeneous texture in the presence of inhomogeneous stress. It can be expected that inhomogeneities in texture will strongly affect Rayleigh-wave dispersion. For the direct problem, where the relevant texture coefficients are known functions of depth, this is not an issue, as we may follow exactly the same procedure as what we did in this section to derive dispersion relations.

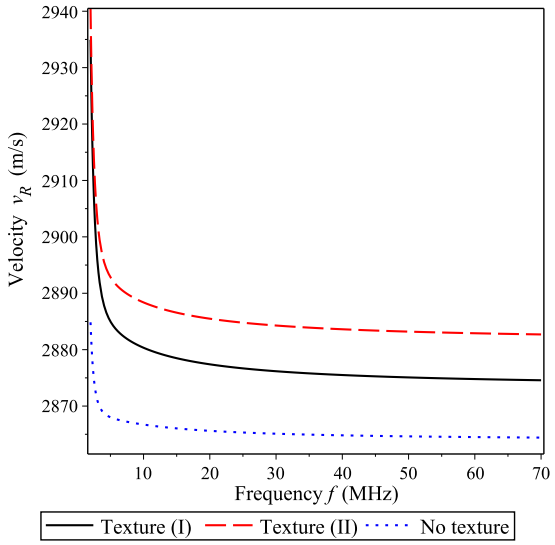

Fig. 7. Dispersion curves for propagation direction $\theta = 90^\circ$.

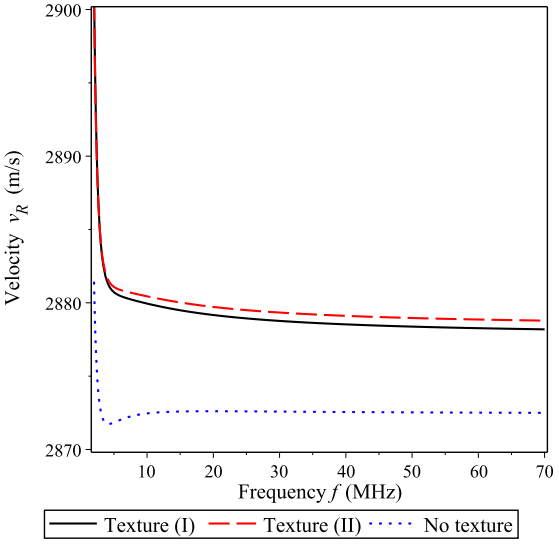

Fig. 8. Dispersion curves for propagation direction $\theta = 135^\circ$.

Table 2
Comparison of first-, second-, and third-order terms in high-frequency asymptotic formula for v_R in 7075-T651 sample.

Texture (I), $\theta = 90^\circ$										
Frequency (MHz)	1	2	3	4	5	6	7	8	10	20
v_1/k (m/s)	100.4	50.2	33.5	25.1	20.1	16.7	14.3	12.5	10.0	5.0
v_2/k^2 (m/s)	−376.3	−94.1	−41.8	−23.5	−15.0	−10.4	−7.7	−5.9	−3.8	−0.9
v_3/k^3 (m/s)	844.7	105.6	31.3	13.2	6.8	3.9	2.5	1.6	0.8	0.1
$v_R - v_0$ (m/s)	568.8	61.7	23.0	14.8	11.9	10.2	9.1	8.2	7.0	4.2

7. Conclusion

In this paper we consider the direct problem of deriving dispersion relations for Rayleigh waves propagating in various directions along the surface of a vertically-inhomogeneous prestressed anisotropic medium when all details about the

prestress and the constitutive equation of the medium are given. For the case where the incremental elasticity tensor can be written as an isotropic part and a perturbative part, we solve the aforementioned problem by deriving necessary formulas to implement the general procedure recently developed by Man et al. (2015) to obtain a high-frequency asymptotic formula for each dispersion relation. We illustrate our solution of the direct problem by deriving dispersion relations for a 7076-T651 aluminum alloy sample with a prestress induced by low plasticity burnishing.

The formulas and procedure presented in this paper can serve as the mathematical foundation of a nondestructive technique that uses the dispersion of Rayleigh waves to monitor changes in the protective prestress placed on metal parts by surface treatments such as low plasticity burnishing.

Acknowledgements

The work of Tanuma was partially supported by Grant-in-Aid for Scientific Research (C), Society for the Promotion of Science, Japan (No. 26400157).

Appendix A. Formulas for ℓ_{ij} in $\mathbf{Z}_0^{\mathbf{Ptb}}(\boldsymbol{v})$

Put

$$P=\frac{1}{\sqrt{(\lambda+2\mu)(\lambda+2\mu-V)}},\quad S=\frac{1}{\sqrt{\mu(\mu-V)}},\quad R=\frac{1}{\sqrt{\mu(\lambda+2\mu)(\mu-V)(\lambda+2\mu-V)}},$$

where λ and μ are the Lamé constants that pertain to $\mathbb{C}^{\mathrm{iso}}$ and $V=\rho(0)\,v^2$. Then

$$\ell_{11}(a_{55},a_{66},\mathring{T}_{22})=\Big((\mu-V)a_{55}+\mu(a_{66}+\mathring{T}_{22})\Big)S/2,$$

$$\begin{aligned}\ell_{22}(a_{22},a_{23},a_{33},a_{44},\mathring{T}_{22})=&\frac{\mu}{2(\lambda+\mu)(\lambda+3\mu-V)^2V}\\&\times\Big[(\lambda+2\mu)\Big((\lambda+2\mu)(\lambda+3\mu)^2-(3\lambda^2+15\lambda\mu+20\mu^2)V+2(\lambda+3\mu)V^2\Big)P\\&-(\mu-V)\Big((\lambda+2\mu)(\lambda+3\mu)^2-(2\lambda^2+11\lambda\mu+13\mu^2)V+(\lambda+\mu)V^2\Big)S\Big]a_{22}\\&+\frac{\mu(\lambda+2\mu-V)}{(\lambda+\mu)(\lambda+3\mu-V)V}\,[-(\lambda+2\mu)(\lambda+3\mu-2V)P+(\lambda+3\mu)(\mu-V)S]a_{23}\\&+\frac{\mu(\lambda+2\mu-V)}{2(\lambda+\mu)(\lambda+3\mu-V)^2V}\,\Big[(\lambda+2\mu-V)\Big((\lambda+3\mu)^2-(3\lambda+7\mu)V\Big)P\\&-(\mu-V)\Big((\lambda+3\mu)^2-(\lambda+5\mu)V\Big)S\Big]a_{33}+\frac{\lambda+2\mu-V}{2(\lambda+\mu)(\lambda+3\mu-V)^2V}\\&\times\Big[-2(\lambda+2\mu)\Big(2\mu(\lambda+3\mu)^2-(\lambda^2+9\lambda\mu+20\mu^2)V+(\lambda+5\mu)V^2\Big)P\\&+\Big(4\mu^2(\lambda+3\mu)^2-2\mu(\lambda^2+11\lambda\mu+22\mu^2)V-(\lambda^2-9\mu^2)V^2+(\lambda+\mu)V^3\Big)S\Big]a_{44}\\&+\frac{\mu}{2(\lambda+3\mu-V)^2}\,\Big[-(\lambda+2\mu)(\lambda+\mu-V)P+\Big(\lambda^2+5\lambda\mu+8\mu^2-(2\lambda+7\mu)V+V^2\Big)S\Big]\mathring{T}_{22},\end{aligned}$$

$$\begin{aligned}\ell_{33}(a_{22},a_{23},a_{33},a_{44},\mathring{T}_{22})=&\frac{(\lambda+2\mu)(\mu-V)}{2(\lambda+\mu)(\lambda+3\mu-V)^2V}\Big[-(\lambda+2\mu)\Big((\lambda+3\mu)^2-(\lambda+5\mu)V\Big)P+\mu\Big((\lambda+3\mu)^2-(3\lambda+7\mu)V\Big)S\Big]a_{22}\\&+\frac{(\lambda+2\mu)(\mu-V)}{(\lambda+\mu)(\lambda+3\mu-V)V}\,[(\lambda+3\mu)(\lambda+2\mu-V)P-\mu(\lambda+3\mu-2V)S]a_{23}\\&+\frac{\mu-V}{2(\lambda+\mu)(\lambda+3\mu-V)^2V}\Big[-(\lambda+2\mu-V)\Big((\lambda+2\mu)(\lambda+3\mu)^2-(2\lambda^2+11\lambda\mu+13\mu^2)V+(\lambda+\mu)V^2\Big)P\\&+\mu\Big((\lambda+2\mu)(\lambda+3\mu)^2-(3\lambda^2+15\lambda\mu+20\mu^2)V+2(\lambda+3\mu)V^2\Big)S\Big]a_{33}\\&+\frac{\lambda+2\mu}{2(\lambda+\mu)(\lambda+3\mu-V)^2V}\Big[2(\lambda+2\mu-V)\Big(2\mu(\lambda+3\mu)^2-(\lambda^2+11\lambda\mu+22\mu^2)V+2(\lambda+3\mu)V^2\Big)P\\&-\Big(4\mu^2(\lambda+3\mu)^2-2\mu(3\lambda^2+21\lambda\mu+38\mu^2)V+(\lambda^2+16\lambda\mu+47\mu^2)V^2-(\lambda+9\mu)V^3\Big)S\Big]a_{44}\\&+\frac{\lambda+2\mu}{2(\lambda+3\mu-V)^2}\,\Big[\Big(2\lambda^2+9\lambda\mu+11\mu^2-(3\lambda+8\mu)V+V^2\Big)P+\mu(\lambda+\mu+V)S\Big]\mathring{T}_{22},\end{aligned}$$

$$\ell_{12}^{\mathrm{R}}(a_{26},a_{36},a_{45}) = \frac{\mu}{2(\lambda+\mu)(\lambda+3\mu-V)V}[(\lambda+2\mu)(\lambda+3\mu)(\lambda+2\mu-V)P-(\mu-V)((\lambda+2\mu)(\lambda+3\mu)-(\lambda+\mu)V)S]a_{26}$$
$$+\frac{\mu(\lambda+2\mu-V)}{2(\lambda+\mu)(\lambda+3\mu-V)V}[-(\lambda+2\mu)(\lambda+3\mu-2V)P+(\lambda+3\mu)(\mu-V)S]a_{36}$$
$$+\frac{\lambda+2\mu-V}{2(\lambda+\mu)(\lambda+3\mu-V)V}[-(\lambda+2\mu)(2\mu(\lambda+3\mu)-(\lambda+5\mu)V)P+(\mu-V)(2\mu(\lambda+3\mu)+(\lambda+\mu)V)S]a_{45},$$

$$\ell_{12}^{\mathrm{I}}(a_{25},a_{35},a_{46}) = \frac{\mu-V}{2(\lambda+\mu)(\lambda+3\mu-V)V}[(\lambda+2\mu)(\lambda+3\mu)-(\lambda+\mu)V-\mu(\lambda+2\mu)(\lambda+3\mu)(\lambda+2\mu-V)R]a_{25}$$
$$+\frac{(\mu-V)(\lambda+2\mu-V)}{2(\lambda+\mu)(\lambda+3\mu-V)V}[-(\lambda+3\mu)+\mu(\lambda+2\mu)(\lambda+3\mu-2V)R]a_{35}$$
$$+\frac{\lambda+2\mu-V}{2(\lambda+\mu)(\lambda+3\mu-V)V}[2\mu(\lambda+3\mu)+(\lambda+\mu)V-\mu(\lambda+2\mu)(2\mu(\lambda+3\mu)-(\lambda+5\mu)V)R]a_{46},$$

$$\ell_{13}^{\mathrm{R}}(a_{25},a_{35},a_{46}) = \frac{(\lambda+2\mu)(\mu-V)}{2(\lambda+\mu)(\lambda+3\mu-V)V}[(\lambda+3\mu)(\lambda+2\mu-V)P-\mu(\lambda+3\mu-2V)S]a_{25}$$
$$+\frac{\mu-V}{2(\lambda+\mu)(\lambda+3\mu-V)V}[-(\lambda+2\mu)(\lambda+2\mu-V)(\lambda+3\mu-2V)P$$
$$+\mu\Big((\lambda+2\mu)(\lambda+3\mu)-2(\lambda+3\mu)V+2V^2\Big)S\Big]a_{35}$$
$$+\frac{\lambda+2\mu}{2(\lambda+\mu)(\lambda+3\mu-V)V}[(\lambda+2\mu-V)(2\mu(\lambda+3\mu)-(\lambda+5\mu)V)P$$
$$-\mu\Big(2\mu(\lambda+3\mu)-(3\lambda+11\mu)V+4V^2\Big)S\Big]a_{46},$$

$$\ell_{13}^{\mathrm{I}}(a_{26},a_{36},a_{45}) = \frac{\mu(\lambda+2\mu)}{2(\lambda+\mu)(\lambda+3\mu-V)V}[-(\lambda+3\mu-2V)+(\lambda+3\mu)(\mu-V)(\lambda+2\mu-V)R]a_{26}$$
$$+\frac{\mu}{2(\lambda+\mu)(\lambda+3\mu-V)V}\Big[(\lambda+2\mu)(\lambda+3\mu)-2(\lambda+3\mu)V+2V^2$$
$$-(\lambda+2\mu)(\mu-V)(\lambda+2\mu-V)(\lambda+3\mu-2V)R]a_{36}$$
$$+\frac{\lambda+2\mu}{2(\lambda+\mu)(\lambda+3\mu-V)V}\Big[2\mu(\lambda+3\mu)-(3\lambda+11\mu)V+4V^2$$
$$-(\mu-V)(\lambda+2\mu-V)(2\mu(\lambda+3\mu)-(\lambda+5\mu)V)R]a_{45},$$

$$\ell_{23}^{\mathrm{R}}(a_{24},a_{34}) = \frac{\lambda+2\mu}{(\lambda+\mu)(\lambda+3\mu-V)V}[(\lambda+2\mu-V)(2\mu(\lambda+3\mu)-(\lambda+4\mu)V)P-\mu(\mu-V)(2(\lambda+3\mu)-3V)S]a_{24}$$
$$+\frac{\lambda+2\mu-V}{(\lambda+\mu)(\lambda+3\mu-V)V}\Big[-(\lambda+2\mu)\Big(2\mu(\lambda+3\mu)-(\lambda+6\mu)V+V^2\Big)P+\mu(\mu-V)(2(\lambda+3\mu)-V)S\Big]a_{34},$$

$$\ell_{23}^{\mathrm{I}}(a_{22},a_{23},a_{33},a_{44},\mathring{T}_{22}) = \frac{\mu(\lambda+2\mu)(\mu-V)}{2(\lambda+\mu)(\lambda+3\mu-V)^2}\big[2-\big(\lambda^2+4\lambda\mu+5\mu^2-(\lambda+3\mu)V\big)R\big]a_{22}$$
$$+\frac{\mu(\mu-V)}{(\lambda+\mu)(\lambda+3\mu-V)}[-1+(\lambda+2\mu)(\lambda+2\mu-V)R]a_{23}$$
$$+\frac{\mu(\mu-V)(\lambda+2\mu-V)}{2(\lambda+\mu)(\lambda+3\mu-V)^2}\big[2-\big(\lambda^2+4\lambda\mu+5\mu^2-(\lambda+3\mu)V\big)R\big]a_{33}$$
$$+\frac{(\lambda+2\mu)(\lambda+2\mu-V)}{2(\lambda+\mu)(\lambda+3\mu-V)^2}\big[-2(\lambda+5\mu-2V)+\big(2\mu(\lambda^2+5\lambda\mu+8\mu^2)$$
$$-(\lambda^2+8\lambda\mu+19\mu^2)V+(\lambda+5\mu)V^2\big)R\big]a_{44}$$
$$+\frac{\mu(\lambda+2\mu)}{2(\lambda+3\mu-V)^2}\big[-2+\big(\lambda^2+4\lambda\mu+5\mu^2-(\lambda+3\mu)V\big)R\big]\mathring{T}_{22}.$$

We have used MATHEMATICA to carry out the computations of some expressions above.

Appendix B. Details on constitutive equation of 7075-T651 aluminum sample

In this appendix we provide the details that complete the constitutive equation (34) of the 7075-T651 sample studied in Section 6.

B.1. Material parameters

In our computations we take $\lambda = 60.79$ GPa and $\mu = 26.9$ GPa, which correspond to the mean values of μ and Young's modulus $E = 71.43$ GPa obtained by Radovic, Lara-Curzio, and Riester (2004) in their RUS (resonant ultrasound spectroscopy) measurements on sixteen 7075-T651 samples. As for the other 10 parameters, we are not aware of any experimentally determined value reported in the literature. In our illustrative example, we adopt the values predicted by the Man–Paroni model (Man, 1999; Man & Paroni, 1996; Paroni & Man, 2000) from second-order and third-order elastic constants of single-crystal pure aluminum reported by Thomas (1968) and Sarma and Reddy (1972), respectively: $\alpha = -16.49$ GPa, $\beta_1 = 0.89, \beta_2 = 0.96, \beta_3 = -2.63, \beta_4 = -4.54, b_1 = -3.32, b_2 = -0.61, b_3 = 0.14, b_4 = 1.54$ and $a = 12.10$.

B.2. Texture coefficients

$W'_{400} = 0.00393, W'_{420} = -0.00083, W'_{440} = -0.00233, W'_{600} = 0.00025, W'_{620} = -0.0004, W'_{640} = -0.00033,$ and $W'_{660} = 0.00035$.

B.3. Components of tensors $\mathbf{\Phi}, \mathbf{\Theta}$, and $\mathbf{\Psi}$

All components of tensors below refer to the coordinate system *OXYZ* defined in Section 6.

An rth order tensor $\boldsymbol{H}$ is said to be harmonic if it is totally symmetric and traceless, i.e., its components $H_{i_1 i_2 \dots i_r}$ satisfy $H_{i_1 i_2 \dots i_r} = H_{i_{\tau(1)} i_{\tau(2)} \dots i_{\tau(r)}}$ for each permutation τ of $\{1, 2, \dots, r\}$, and $\mathrm{tr}_{j,k}\boldsymbol{H} = \boldsymbol{0}$ for any pair of distinct indices j and k. For example, for $r = 3$ we have $H_{112} = H_{121} = H_{211}$, etc. from total symmetry, and $H_{111} + H_{212} + H_{313} = 0$, etc. from the traceless condition.

The fourth-order tensor $\mathbf{\Phi}$ and the sixth-order tensor $\mathbf{\Theta}$ are harmonic. All the non-trivial components of $\mathbf{\Phi}$ can be obtained from the following five through the total symmetry of and the traceless condition on the harmonic tensor $\mathbf{\Phi}$:

$$\Phi_{1122} = W'_{400} - \sqrt{70}\,W'_{440}\cos 4\theta, \quad \Phi_{1133} = -4W'_{400} + 2\sqrt{10}\,W'_{420}\cos 2\theta,$$
$$\Phi_{2233} = -4W'_{400} - 2\sqrt{10}\,W'_{420}\cos 2\theta, \quad \Phi_{1112} = -\sqrt{10}\,W'_{420}\sin 2\theta + \sqrt{70}\,W'_{440}\sin 4\theta,$$
$$\Phi_{2212} = -\sqrt{10}\,W'_{420}\sin 2\theta - \sqrt{70}\,W'_{440}\sin 4\theta.$$

The non-trivial components of $\mathbf{\Theta}$ can be obtained from the following seven by using the total symmetry of and the traceless condition on $\mathbf{\Theta}$:

$$\Theta_{222211} = -W'_{600} - \frac{\sqrt{105}}{15}W'_{620}\cos 2\theta + \sqrt{14}\,W'_{640}\cos 4\theta + \sqrt{231}\,W'_{660}\cos 6\theta,$$
$$\Theta_{222233} = 6W'_{600} + \frac{16\sqrt{105}}{15}W'_{620}\cos 2\theta + 2\sqrt{14}\,W'_{640}\cos 4\theta,$$
$$\Theta_{333311} = -8W'_{600} + \frac{16\sqrt{105}}{15}W'_{620}\cos 2\theta, \quad \Theta_{333322} = -8W'_{600} - \frac{16\sqrt{105}}{15}W'_{620}\cos 2\theta,$$
$$\Theta_{122222} = \frac{\sqrt{105}}{3}W'_{620}\sin 2\theta + 2\sqrt{14}\,W'_{640}\sin 4\theta + \sqrt{231}\,W'_{660}\sin 6\theta,$$
$$\Theta_{122233} = -\frac{8\sqrt{105}}{15}W'_{620}\sin 2\theta - 2\sqrt{14}\,W'_{640}\sin 4\theta, \quad \Theta_{123333} = \frac{16\sqrt{105}}{15}W'_{620}\sin 2\theta.$$

The components of the sixth-order tensors $\mathbf{\Psi}^{(i)}(w)$ are given in terms of those of the harmonic tensor $\mathbf{\Phi}$ by the following formulae:

$$\Psi^{(1)}_{ijklmn} = \Phi_{ijkl}\delta_{mn}, \quad \Psi^{(2)}_{ijklmn} = \Phi_{klmn}\delta_{ij} + \Phi_{ijmn}\delta_{kl},$$
$$\Psi^{(3)}_{ijklmn} = \delta_{ik}\Phi_{jlmn} + \delta_{il}\Phi_{jkmn} + \delta_{jk}\Phi_{ilmn} + \delta_{jl}\Phi_{ikmn},$$
$$\Psi^{(4)}_{ijklmn} = \delta_{im}\Phi_{jnkl} + \delta_{in}\Phi_{jmkl} + \delta_{jm}\Phi_{inkl} + \delta_{jn}\Phi_{imkl} + \delta_{km}\Phi_{lnij} + \delta_{kn}\Phi_{lmij} + \delta_{lm}\Phi_{knij} + \delta_{ln}\Phi_{kmij},$$

where δ_{ij} is the Kronecker delta.

References

Aluminum Standards and Data 2000 (2000). Washington, DC: The Aluminum Association.
Bellman, R. (1997). *Introduction to matrix analysis* (2nd ed.). Philadelphia: SIAM.
Biot, M. A. (1965). *Mechanics of incremental deformations*. New York: John Wiley.

Chadwick, P., & Smith, G. D. (1977). Foundations of the theory of surface waves in anisotropic elastic materials. *Advances in Applied Mechanics, 17*, 303–376.
Gantmacher, F. R. (1960). *The theory of matrices*. Providence, Rhode Island: American Mathematical Society.
Hoger, A. (1986). On the determination of residual stress in an elastic body. *Journal of Elasticity, 16*, 303–324.
Katchalov, A. P. (2012). Rayleigh waves in an anisotropic elastic medium and impedance. *Journal of Mathematical Sciences, 185*, 581–590.
Lothe, J., & Barnett, D. M. (1976). On the existence of surface-wave solutions for anisotropic elastic half-spaces with free surface. *Journal of Applied Physics, 47*, 428–433.
Man, C.-S. (1999). Effects of crystallographic texture on the acoustoelastic coefficients of polycrystals. *Nondestructive Testing and Evaluation, 15*, 191–214.
Man, C.-S., & Carlson, D. E. (1994). On the traction problem of dead loading in linear elasticity with initial stress. *Archive for Rational Mechanics and Analysis, 128*, 223–247.
Man, C.-S., & Lu, W. Y. (1987). Towards an acoustoelastic theory for measurement of residual stress. *Journal of Elasticity, 17*, 159–182.
Man, C.-S., Lu, W.-Y., & Li, J. (1999). Effects of crystallographic texture on the acoustoelastic coefficients for Rayleigh waves in aluminum. In D. O. Thompson & D. E. Chimenti (Eds.). *Review of progress in quantitative nondestructive evaluation* (18, pp. 1879–1886). New York: Kluwer.
Man, C.-S., Nakamura, G., Tanuma, K., & Wang, S. (2015). Dispersion of Rayleigh waves in vertically-inhomogeneous prestressed elastic media. *IMA Journal of Applied Mathematics, 80*, 47–84.
Man, C.-S., & Paroni, R. (1996). On the separation of stress-induced and texture-induced birefringence in acoustoelasticity. *Journal of Elasticity, 45*, 91–116.
Moreau, A., & Man, C.-S. (2006). Laser-ultrasonic measurements of residual stresses in a 7075-T651 aluminum sample surface-treated with low plasticity burnishing. In D. O. Thompson & D. E. Chimenti (Eds.). *Review of progress in quantitative nondestructive evaluation* (25, pp. 1434–1441). Melville, New York: American Institute of Physics.
Paroni, R., & Man, C.-S. (2000). Two micromechanical models in acoustoelasticity: A comparative study. *Journal of Elasticity, 59*, 145–173.
Radovic, M., Lara-Curzio, E., & Riester, L. (2004). Comparison of different experimental techniques for determination of elastic properties of solids. *Materials Science and Engineering A, 368*, 56–70.
Sarma, V. P. N., & Reddy, P. J. (1972). Third-order elastic constants of aluminum. *Physica Status Solidi (a), 10*, 563–567.
Song, Y. Q., & Fu, Y. B. (2007). A note on perturbation formulae for the surface-wave speed due to perturbations in material properties. *Journal of Elasticity, 88*, 187–192.
Thomas, J. F. (1968). Third order elastic constants of aluminum. *Physical Review, 175*, 955–962.
Tanuma, K., & Man, C.-S. (2002). Angular dependence of Rayleigh-wave velocity in prestressed polycrystalline media with monoclinic texture. *Journal of Elasticity, 69*, 181–214.
Tanuma, K., & Man, C.-S. (2006). Perturbation formula for phase velocity of Rayleigh waves in prestressed anisotropic media. *Journal of Elasticity, 85*, 21–37.
Tanuma, K., & Man, C.-S. (2008). Perturbation formulas for polarization ratio and phase shift of Rayleigh waves in prestressed anisotropic media. *Journal of Elasticity, 92*, 1–33.
Tanuma, K., Man, C.-S., & Du, W. (2013). Perturbation of phase velocity of Rayleigh waves in pre-stressed anisotropic media with orthorhombic principal part. *Mathematics and Mechanics of Solids, 18*, 301–322.
Ting, T. C. T. (1996). *Anisotropic elasticity*. New York: Oxford University Press.